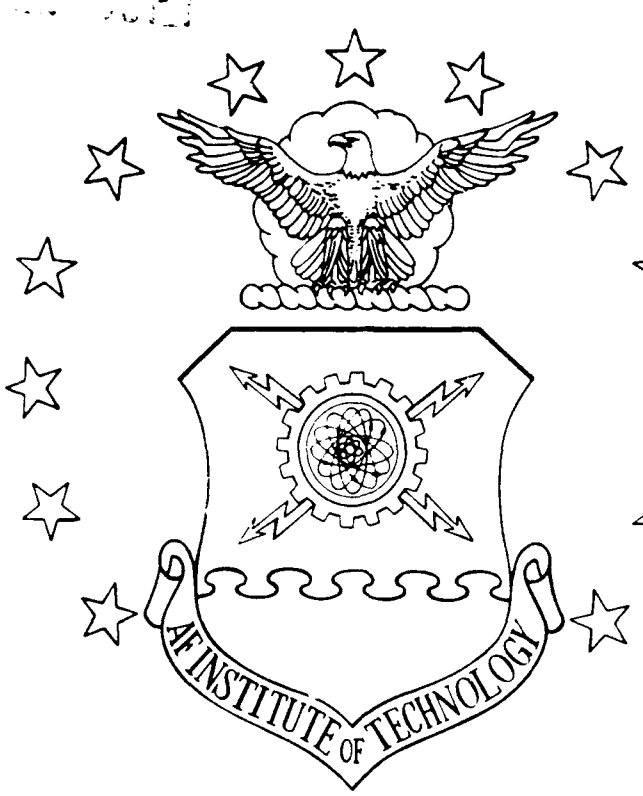

H_2 AND H_∞ OPTIMIZATION WITH A RESTRICTED REGION OF STABILITY

THESIS

Michael J. Mares, Captain, USAF

AFIT/GAE/ENY/90D-15

DEPARTMENT OF THE AIR FORCE
AIR UNIVERSITY
AIR FORCE INSTITUTE OF TECHNOLOGY

Wright-Patterson Air Force Base, Ohio

AFIT/GAE/ENY/90D-15

(1)

H_2 AND H_∞ OPTIMIZATION WITH A RESTRICTED REGION OF STABILITY

THESIS

Michael J. Mares, Captain, USAF

AFIT/GAE/ENY/90D-15

AFIT/GAE/ENY/90D-15

H_2 AND H_∞ OPTIMIZATION WITH A RESTRICTED REGION OF STABILITY

THESIS

Presented to the Faculty of the School of Engineering
of the Air Force Institute of Technology
Air University
In Partial Fulfillment of the
Requirements for the Degree of
Master of Science in Aeronautical Engineering

Michael J. Mares, B.S.
Captain, USAF

December 1990

Acknowledgments

In understanding the theory, deriving the equations, performing the experimentation and writing this thesis I am deeply indebted to my faculty advisor, Captain D. Brett Ridgely. The concept for the work here, as well as much of Chapter 4, is based on his ideas. I would also like to thank my thesis committee, Dr. Liebst and Lt Col Bagley.

Table of Contents

Page

Acknowledgements ii

List of Figures v

List of Tables viii

Abstract ix

1. Introduction 1

2. H_2 and H_∞ Control Design Methods 3
   2.1. Block Diagram and State Space Equations 3
   2.2. Properties and Equations of H_2 and H_∞ Optimization 6
      2.2.1. H_2 Optimization. 6
      2.2.2. H_∞ Optimization. 9

3. Previous S-plane Transformations 12
   3.1. Closed-Loop Poles Left of a Vertical Line 13
   3.2. Closed-Loop Poles Inside a Cone 17

4. Plane Transformations 21
   4.1. α Shift 21
   4.2. ζ Rotation 23
      4.2.1. Cylindrical Coordinates. 23
      4.2.2. Cartesian Coordinates. 26
   4.3. Combined α Shift and ζ Rotation 28
   4.4. Effects of the Transformation on a Vertical Line 30

5. State Space Equations for the α Shift 34

6. Example Problem 1 37
   6.1. Block Diagrams and Generalized State Space Equations 37
   6.2. Numerical Values for the System Used 41
   6.3. Closing the Loop 44
   6.4. Mechanics of the α Shift 47
   6.5. Results for H_2 Optimization 48
      6.5.1. $\alpha = 0$ (Original Plant). 48

6.5.2. $\alpha = 1.5$ (Unstable). 50
6.5.3. $\alpha = 2.5$ (Unstable and Nonminimum Phase). ... 52
6.5.4. Conclusions for H_2 Optimization. 54
6.6. Results for H_∞ Optimization 57

7. Example Problem 2 59
7.1. Problem Statement 59
7.2. H_2 Optimization Setup and Equations 61
7.3. H_2 Optimization with no α Shift 66
7.4. H_2 Optimization with an α Shift of 0.3 73

8. Perturbing the Plant 82
8.1. Perturbation Number 1 83
8.1.1. Perturbation Number 1 with no α Shift. ... 84
8.1.2. Perturbation Number 1 with 0.3 α Shift. .. 88
8.2. Perturbation Number 2 93

9. Results and Conclusions 96
9.1. Summarizing the Example Problems 96
9.2. Conclusions 98
9.2.1. Areas for Further Study. 98

Bibliography 101

Vita 103

List of Figures

Figure		Page
1	Block diagram for general feedback	4
2	Approximating a cone in the LHP with a hyperbola	18
3	α shift	22
4	ζ rotation	24
5	Slopes for θ transformation	26
6	Combined α shift and ζ rotation	29
7	Line before coordinate transformation	31
8	Line after ζ rotation	32
9	Line after a combined transformation	32
10	Block diagram for Example 1 with weightings	37
11	Singular value plot of weighting factor	43
12	Block diagram feedback format	45
13	Block diagram for Example 1 with command input	45
14	Sensitivity of Example 1 with no α shift	49
15	Control usage with no α shift	49
16	Response to a command input with no α shift	50
17	Sensitivity for Example 1 with 1.5 α shift	51
18	Control usage with 1.5 α shift	52
19	Response to a command input with 1.5 α shift	52
20	Sensitivity for Example 1 with 2.5 α shift	53
21	Control usage with 2.5 α shift	54

22 Response to a command input with 2.5 α shift 54

23 Block diagram for design on Example 2 62

24 Block diagram feedback format 64

25 Block diagram for Example 2 with command input 65

26 Sensitivity for Example 2 with no α shift 66

27 Control power for step sideslip angle 67

28 Control power for step roll angle 68

29 Rejecting a sideslip disturbance 68

30 Rejecting a roll disturbance 69

31 Response to a sideslip command 70

32 Response to a roll command 70

33 Poles and zeros for the $\alpha = 0$ case 72

34 Sensitivity for Example 2 with 0.3 α shift 75

35 Control power for sideslip angle command 76

36 Control power for roll angle command 76

37 Rejecting a sideslip disturbance 77

38 Rejecting a roll angle disturbance 78

39 Response to a sideslip command 79

40 Response to a roll command 79

41 Poles and zeros for $\alpha = 0.3$ case 81

42 Sensitivity for perturbation 1 with no α shift 85

43 Control power for sideslip command 85

44 Control power for a roll command 86

45 Rejecting a sideslip disturbance 86

46 Rejecting a roll disturbance 87
47 Response to a sideslip command 87
48 Response to a roll command 88
49 Sensitivity for perturbation 1 with 0.3 α shift 89
50 Control power for sideslip command 90
51 Control power for a roll command 90
52 Rejecting a sideslip disturbance 91
53 Rejecting a roll disturbance 91
54 Response to a sideslip command 92
55 Response to a roll command 92
56 Combined s-plane transformation 100

List of Tables

		Page
1	H_2 optimization results for Example 1	55
2	Closed loop poles and zeros for Example 1	56
3	H_∞ results for Example 1	58
4	Open loop poles for Example 2	61
5	Closed-loop poles and zeros for Example 2, no shift	72
6	H_2 optimization results for Example 2	74
7	Closed-loop poles and zeros for Example 2, 0.3 shift	80
8	Open loop poles for Example 2, no perturbation	83
9	Open loop poles for Example 2, perturbation 1	84
10	Open loop poles for Example 2, perturbation 2	93
11	Summary of perturbation effects	95

Abstract

Many modern control design methods, such as H_2 and H_∞ optimization, guarantee that the closed loop system will be stable. To make further use of this guarantee, the portion of the s-plane considered to be stable is restricted to a region left of a vertical line some distance α from the imaginary axis. This α shift was accomplished in the state space equations, so standard computational tools still work. Now the system is not only guaranteed to be stable, but also has some guaranteed speed for the time response. The equations for guaranteeing some arbitrary damping ratio were also derived in Cartesian coordinates, but only the α shift was put into the state space equation form and tested. The α shift increased the speed of the system, as expected. An additional benefit was increasing the damping of lightly damped poles. The cost for doing this was an increase in the steady state error and an increase in the control power required. The α shift is very easy to perform in the state space equations. The bottom line is that it gives the design engineer another parameter to adjust to get better system performance.

H_2 AND H_∞ OPTIMIZATION WITH A RESTRICTED REGION OF STABILITY

1. Introduction

Many modern control design methods guarantee stability, i.e. that all the closed-loop poles are in the Left Half Plane (LHP). Since stability is insured by the mathematics of the design procedure, the design engineer can focus his attention on achieving other design parameters. Rather than just guaranteeing stability it would be beneficial to insure other parameters, such as a minimum speed of response and a minimum damping ratio. This could be accomplished by restricting the region of the s-plane considered to be stable. This thesis will present a method for transforming the "stable" region of the s-plane to an area left of a vertical line some distance α to the left of the imaginary axis. Shifting all the closed-loop poles away from the imaginary axis will increase the speed of the system and will increase the damping of complex poles that are close to

the imaginary axis.

Chapter 2 presents the equations and design methodology for H_2 and H_∞ optimization. It also gives some of the properties and uses for each. Chapter 3 gives an overview of the previous work in this area. Since H_2 and H_∞ optimization are so recent, the earlier work was for designing Linear Quadratic Regulators (LQR). Chapter 4 presents the mathematics for transforming the complex plane. Besides the α shift, it shows the equations for rotating the imaginary axis by some angle ζ. This transformation will guarantee some minimum damping ratio. Chapter 5 shows the state space representation of the α shift. Chapters 6 and 7 are example problems. The first one is a simple plant that shows the effect of shifting the imaginary axis across open-loop poles and zeros. The second example is for a drone aircraft. It shows how the α shift can be used to increase the damping of a system with complex poles near the imaginary axis. Chapter 8 shows how the α shift affects robustness. The compensator that was designed for the original plant is tested on several perturbed plants. Chapter 9 gives the conclusions and recommendations for areas of further study.

2. H_2 and H_∞ Control Design Methods

Classical control design methods, such as root locus and Bode plots, work very well on simple Single Input Single Output (SISO) systems. As the system becomes more complex, however, new design methods are needed. For a complex SISO system simply feeding back the gain or adding filters may not be enough to achieve the desired closed-loop response and for Multiple Input Multiple Output (MIMO) systems the classical methods are not easy to use at all. The following discussion on modern control design methods is not meant to be complete or quantitative. The interested reader is referred to [4], [5], [8] and [10] for complete discussion and mathematical derivations. H_2 and H_∞ optimization will be the only methods discussed here. Linear Quadratic Gaussian (LQG) is in the category of modern control, and is a special case of H_2 optimization.

2.1. Block Diagram and State Space Equations

Consider the block diagram in Figure 1.

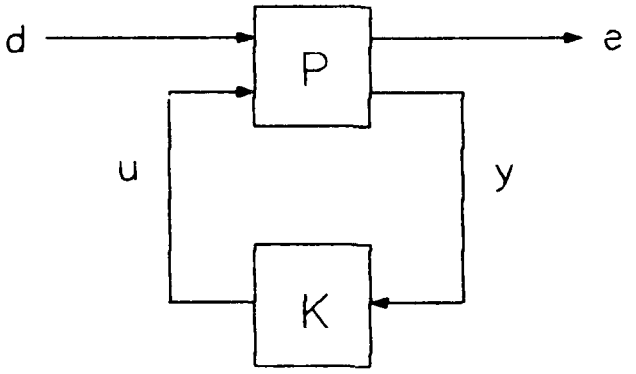

Figure 1 General feedback block diagram

The state space equations for the system are

$$\dot{x} = Ax + B_d d + B_u u \tag{1}$$

$$e = C_e x + D_{ed} d + D_{eu} u \tag{2}$$

$$y = C_y x + D_{yd} d + D_{yu} u \tag{3}$$

The following are also required:

(A, B_d) stabilizable and (C_e, A) detectable (4)

(A, B_u) stabilizable and (C_y, A) detectable (5)

Also, assume that

$$D_{ed} = 0 \text{ and } D_{yu} = 0 \tag{6}$$

$$D_{eu}^T D_{eu} = I \text{ and } D_{yd} D_{yd}^T = I \tag{7}$$

To satisfy the assumption in Equation (7), y and u must be scaled. The rescaled equations are

$$u = S_u^{-1} \bar{u} \tag{8}$$

$$\tilde{y} = S_y y \tag{9}$$

where S_u and S_y are found from

$$S_u^T S_u = D_{eu}^T D_{eu} \tag{10}$$

$$S_y^{-1} (S_y^{-1})^T = D_{yd} D_{yd}^T \tag{11}$$

by using a Cholesky decomposition. The scaled state space equations become

$$\dot{x} = Ax + B_d d + \bar{B}_u \bar{u} \tag{12}$$

$$e = C_e x + \bar{D}_{eu} \bar{u} \tag{13}$$

$$\bar{y} = \bar{C}_y x + \bar{D}_{yd} d \tag{14}$$

where

$$\bar{B}_u = B_u S_u^{-1} \qquad \bar{C}_y = S_y C_y \tag{15}$$

$$\bar{D}_{eu} = D_{eu} S_u^{-1} \qquad \bar{D}_{yd} = S_y D_{yd} \tag{16}$$

The above notation will be used for the remainder of this chapter. What follows is known as the Doyle/Glover parameterization of H_2 and H_∞ optimal compensators.

2.2. Properties and Equations of H_2 and H_∞ Optimization

2.2.1. H_2 Optimization.

H_2 optimization begins with the family of all stabilizing compensators K, and finds the one that minimizes the 2 norm of the closed-loop transfer function, T_{ed}. The 2 norm is defined as

$$\|T_{ed}\|_2 = \left(\frac{1}{2\pi} \int_{-\infty}^{\infty} tr[T_{ed}(j\omega)^* T_{ed}(j\omega)] d\omega \right)^{\frac{1}{2}} \tag{17}$$

The H_2 optimal compensator is given by

$$K = -K_c(sI - A_k)^{-1} K_f \tag{18}$$

where

$$A_k = A - K_f \bar{C}_y - \bar{B}_u K_c \tag{19}$$

$$K_c = \bar{B}_u^T X_2 + \bar{D}_{eu}^T C_e \tag{20}$$

$$K_f = Y_2 \bar{C}_y^T + B_d \bar{D}_{yd}^T \tag{21}$$

X_2 and Y_2 are the solutions to the following Riccati equations:

$$(A - \bar{B}_u \bar{D}_{eu}^T C_e)^T X_2 + X_2(A - \bar{B}_u \bar{D}_{eu}^T C_e) - X_2 \bar{B}_u \bar{B}_u^T X_2 + C_1^T C_1 = 0 \tag{22}$$

where

$$C_1 = (I - \bar{D}_{eu}\bar{D}_{eu}^T)C_e \tag{23}$$

and

$$(A - B_d\bar{D}_{yd}^T\bar{C}_y)Y_2 + Y_2(A - B_d\bar{D}_{yd}^T\bar{C}_y)^T - Y_2\bar{C}_y^T\bar{C}_yY_2 + B_1B_1^T = 0 \tag{24}$$

where

$$B_1 = B_d(I - \bar{D}_{yd}^T\bar{D}_{yd}) \tag{25}$$

Another way to think of H_2 optimization is to minimize the area under the Singular Value (SV) plot of the closed-loop transfer function. Obviously, the SV plot must approach 0 as ω approaches ∞ or the 2 norm will be infinite. This is the reason that the D_{ed} must be 0. If it is anything but 0 the closed-loop system will not be strictly proper, and the SV plot will not approach 0 as the frequency approaches ∞. The H_2 control design method is most effective on a system with a white noise input. It will design a compensator K that minimizes the energy of the output based on a white noise input and the amount of control power allowed. H_2 optimization is also good for reducing the effects of parameter variations.

2.2.2. H_∞ Optimization.

H_∞ optimization begins with the family of all stabilizing compensators K, and finds one that minimizes the ∞ norm of the closed-loop transfer function, T_{cl}. Unlike H_2 optimization, the solution to H_∞ optimization is not unique. The ∞ norm is defined as

$$|T_{cl}|_\infty = \sup_\omega \sigma_{max}[T_{cl}(j\omega)] \tag{26}$$

where σ_{max} is the maximum singular value.

The central member of the family of all stabilizing compensators such that

$$|T_{cl}|_\infty \leq \gamma \tag{27}$$

is given by

$$K = -K_c(sI - A_k)^{-1}K_f \tag{28}$$

where

$$A_k = A - K_f \bar{C}_y - \bar{B}_u K_c + \gamma^{-2} Y_- C_e^T (C_e - \bar{D}_{eu} K_c) \tag{29}$$

$$K_c = (\bar{B}_u^T X_- + \bar{D}_{eu}^T C_e)(I - \gamma^{-2} Y_- X_-)^{-1} \tag{30}$$

$$K_f = Y_- \bar{C}_y^T + B_d \bar{D}_{yd}^T \tag{31}$$

X_- and Y_- are the solutions to the following Riccati equations:

$$(A - \bar{B}_u \bar{D}_{eu}^T C_e)^T X_- + X_-(A - \bar{B}_u \bar{D}_{eu}^T C_e) - X_-(\bar{B}_u \bar{B}_u^T - \gamma^{-2} B_d B_d^T) X_- + C_1^T C_1 = 0 \tag{32}$$

where

$$C_1 = (I - \bar{D}_{eu} \bar{D}_{eu}^T) C_e \tag{33}$$

and

$$(A - B_d \bar{D}_{yd}^T \bar{C}_y) Y_- + Y_-(A - B_d \bar{D}_{yd}^T \bar{C}_y)^T - Y_-(\bar{C}_y^T \bar{C}_y - \gamma^{-2} C_e^T C_e) Y_- + B_1 B_1^T = 0 \tag{34}$$

where

$$B_1 = B_d (I - \bar{D}_{yd}^T \bar{D}_{yd}) \tag{35}$$

For this to be a valid parameterization, the following three conditions must be met:

$$X_{\infty} \geq 0 \tag{36}$$

$$Y_{\infty} \geq 0 \tag{37}$$

$$\rho(Y_{\infty} X_{\infty}) \leq \gamma^2 \tag{38}$$

where $\rho(\cdot)$ is the spectral radius.

The H_{∞} optimization equations must be iterated. If any of the above conditions fail, γ must be increased. If all of them pass γ can be decreased. By doing this repeatedly, γ can be brought arbitrarily close to the optimal value.

From the definition (Equation 26) it is clear that the ∞ norm is simply the peak value of the maximum SV of the closed-loop transfer function. H_{∞} optimization has two main uses. First, it will minimize the energy of the output to an unknown, but bounded energy input. Second, it will minimize the effects of unmodelled dynamics and structural uncertainties, i.e. robustness.

3. Previous S-plane Transformations

The previous chapter discussed some of the advantages of the H_2 and H_∞ optimization design methods. One of the important properties is their guaranteed stability. Many researchers have tried to expand on this point. If all the closed-loop poles can be forced to be left of the imaginary axis, why can't they be restricted to some subset of the left half plane? This chapter will examine some of the schemes put forward to make further restrictions on the location of the poles. Basically, the restrictions are one of two kinds. First, move all the poles some minimum distance from the imaginary axis; i.e. left of a vertical line. Second, move only the lightly damped poles away from the imaginary axis, or at least move them more than the poles with better damping. The first kind will increase the stability and speed of the system and the second kind will increase the damping ratio. Previous works have examined the theory for restricting the region of stability for the Linear Quadratic Regulator (LQR) design. The following is a brief description of some of their techniques.

3.1. Closed-Loop Poles Left of a Vertical Line

The first effort to restrict the region considered to be stable was put forward by Anderson and Moore in 1969 ([2] and [3]). To make it easier to follow, their equations have been put into standard notation.

They begin with the time-invariant linear system

$$\dot{x} = Ax + Bu \tag{39}$$

$$u = -K^T x \tag{40}$$

subject to the following performance index

$$J = \int_{t_0}^{\infty} (u^T R u + x^T Q x) dt \tag{41}$$

where R is a positive definite symmetric constant matrix and Q is a nonnegative definite symmetric constant matrix.

To get the desired pole movement they replace the performance index with

$$J = \int_{t_0}^{\infty} (u^T R u + x^T Q x) e^{2\alpha t} dt \tag{42}$$

where α is the desired minimum distance left of the imaginary axis. Next let

$$\hat{x} = xe^{\alpha t} \tag{43}$$

$$\hat{u} = ue^{\alpha t} \tag{44}$$

Substituting into the performance index

$$J = \int_{t_0}^{\infty} (\hat{u}^T R\hat{u} + \hat{x}^T Q\hat{x})dt \tag{45}$$

If the eigenvalue corresponding to any state x does not decay at least as fast as $e^{-\alpha t}$, J will be infinite. In other words, the real part of each closed-loop eigenvalue must be left of $-\alpha$.

The new state equation becomes

$$\dot{\hat{x}} = (A + \alpha I)\hat{x} + B\hat{u} \tag{46}$$

The new state equation is very similar to the original. A is replaced with $A+\alpha I$ and everything else remains the same. Anderson and Moore then examined some of the properties of the shifted system.

In 1985 Amin [1] used the principle discovered by Anderson and Moore, along with pole placement techniques, to devise a method of shifting the real parts of the open-loop poles to any desired position without affecting the imaginary parts. His approach moved each pole or complex pair individually and could be used iteratively to move any number of poles. His solution was based on solving either a first or second order Lyapunov equation; no (non-linear) algebraic Riccati equations are involved. This approach would be useful if it is important that the imaginary part of the pole not change.

In 1986, Sheieh, Dib, and Mcinnis [12] presented a method for restricting the closed-loop poles to a vertical strip in the LHP. They began with the standard system, performance index and control law given by

$$\dot{x} = Ax + Bu \tag{47}$$

$$J = \int_0^\infty (u^T R u + x^T Q x) dt \tag{48}$$

$$u = -Kx = -R^{-1} B^T P x \tag{49}$$

where P is the solution to the algebraic Riccati equation

$$PA + A^T P + Q - PBR^{-1} B^T P = 0 \tag{50}$$

The optimal closed-loop system is

$$\dot{x} = (A - BK)x \tag{51}$$

They showed that the closed-loop system can be designed to be

$$\dot{x} = (A - rBK)x \tag{52}$$

where

$$r = \frac{1}{2} + \frac{h_2 - h_1}{tr(BK)} \tag{53}$$

and h_1 and h_2 are the distances from the imaginary axis to the left and right sides of the vertical strip, respectively. This method not only moves all the poles left of some line, but also restricts them from being too far to the left. It would be useful on systems with two time scales, one fast and one slow.

3.2. Closed-Loop Poles Inside a Cone

In 1983, Kawasaki and Shimemura [7] designed an iterative method to choose the quadratic weights in LQR. They approximated a 45 degree cone in the LHP with the hyperbola (see Figure 2)

$$(Re\lambda)^2 - (Im\lambda)^2 = m^2 \tag{54}$$

Using the standard state equation and quadratic cost function they first solve the standard LQR problem.

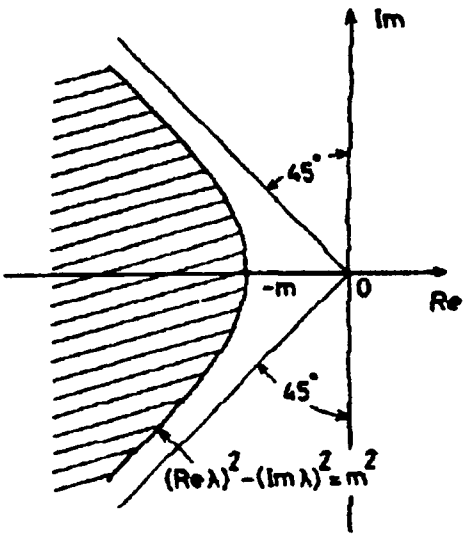

Figure 2 Approximating a conic sector in the LHP with a hyperbola

Next, beginning with the standard solution, they iterate the following equations until K_i is equal to zero. Let

$$A_i = A_{i-1} - BR^{-1}B^T P_i^* \tag{55}$$

where i = 1,2,... and $A_0 = A$

Next, solve the following equation for K_i^* (the superscript + denotes the maximum solution)

$$K_i B R^{-1} B^T K_i + K_i (A_i^2 - m^2 I) + (A_i^2 - m^2 I)^T K_i = 0 \tag{56}$$

If $K_i^* = 0$, then the solution is complete. If $K_i^* \neq 0$ then choose some arbitrary real number r_i such that $r_i > \frac{1}{2}$ and calculate P_{i+1}^* of the following equation

$$P_{i+1} B R^{-1} B^T P_{i+1} - P_{i+1} A_i - A_i^T P_{i+1} - r_i K_i^* = 0 \tag{57}$$

Next, solve for $A_{i+1} = A_i - B R^{-1} B^T P_{i+1}^*$, the closed-loop system matrix, and go back to Equation (55).

The final closed-loop system is

$$A - B R^{-1} B^T (P_1^* + P_2^* + \ldots + P_j^*) \tag{58}$$

where P_j^* is the solution to Equation (57) for $K_i^* = 0$.

The above closed-loop system has all it's eigenvalues in the hatched region of Figure 2.

Next, in 1988, Sheieh, Dib, and Mcinnis [11] presented a method to restrict the closed-loop poles to a cone with either a 45 degree or 30 degree angle from the negative real axis. Again they begin with the standard state equation and quadratic cost function. Their method is an iterative

method similar to the one presented by Kawasaki and Shimemura. The details and specific design steps are in [11].

One additional paper is worth mentioning. In 1984, Oliver [9] presented a scheme for restricting the region of stability to any region symmetric about the real axis. While this method is general, it would be hard to implement in anything other than very simple cases.

4. Plane Transformations

4.1. α Shift

H_2 and H_∞ optimization are extremely powerful compensator design methods. They guarantee that the closed-loop system is stable and minimizes either the 2 norm or the ∞ norm, respectively, of the closed-loop transfer function. The stability guarantee is particularly useful. It says that all the closed-loop poles will be to the left of the imaginary axis. For example, a plant with a pole and a zero in the right half plane (unstable and non-minimum phase) will become closed-loop stable. Regardless of where the pole and zero are in the right half plane, H_2 or H_∞ optimization designs a compensator that places all the closed-loop poles in the left half plane. Rather than just placing all the poles in the left half plane, it may be useful to place them to the left of a vertical line some distance α from the imaginary axis. This will insure that the closed-loop system is not only stable, but has some specified degree of stability. Looking at this from the time domain, it will insure that the system has some guaranteed speed of response. Figure 3 shows the α shift in Cartesian coordinates. For the equations in this section

the variable with the bar above it is the transformed variable. For example, x is the original coordinate and $\bar{x}$ is the transformed coordinate.

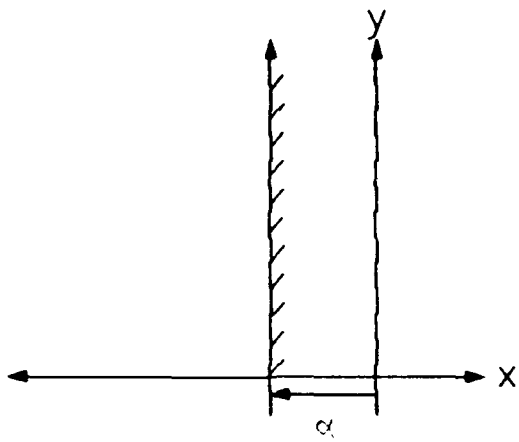

Figure 3 Alpha shift

The equations for this plane transformation are simply

$$\bar{y} = y \tag{59}$$

$$\bar{x} = x + \alpha \tag{60}$$

The next logical step is to transform these equations to the s-plane and finally to state space equations. Almost all modern control design calculations, including H_2 and H_∞ optimization, are performed on state space equations. The next chapter will show the manipulations required to transform the state space equations to accomplish an α shift. Before that, however, some other useful transformations on the s-plane stable region will be shown.

4.2. ζ Rotation

As shown in Section 4.1, transforming the left half plane to a sub-plane left of a vertical line some distance α from the imaginary axis is not very difficult. Another useful transformation would be to rotate the imaginary axis by some angle into the left half plane. Forcing all the closed-loop poles to lie in this restricted region will guarantee that the system will have some minimum damping ratio.

4.2.1. Cylindrical Coordinates.

The first step is to show the rotation in cylindrical coordinates. For this transformation, r (the distance from the origin) is held constant. Figure 4 shows the rotation of the imaginary axis. γ is the angle from the negative

real axis to the desired imaginary axis location and θ is the angle from the positive real axis to the point of interest.

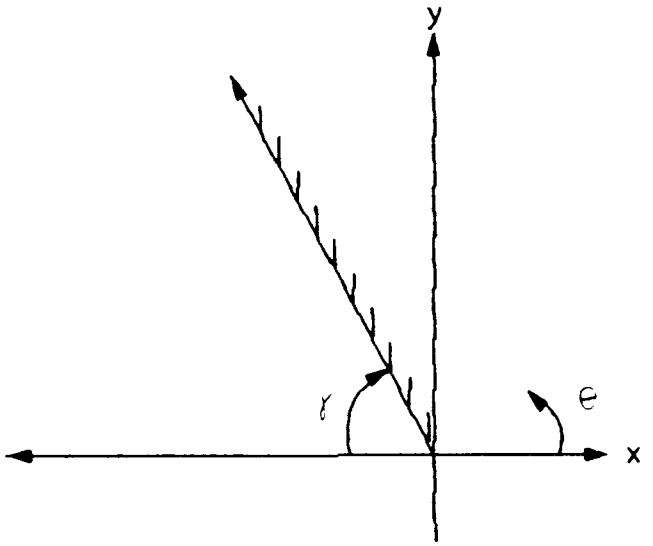

Figure 4 Rotating the imaginary axis to some damping ratio

The following equation relates γ to the damping ratio ζ

$$\gamma = \cos^{-1}\zeta \tag{61}$$

θ is the angle from the positive real axis before the transformation and $\bar{\theta}$ is the angle after transformation.

If $\theta = 180° - \gamma$, then $\bar{\theta} = 90°$

If $\theta = 0°$, then $\bar{\theta} = 0°$

If $\theta = 180°$, then $\bar{\theta} = 180°$

Figure 5 shows how θ is related to $\bar{\theta}$. Each line at angle θ from the positive real axis is rotated to some angle $\bar{\theta}$ by the following equations.

$$\theta \leq 180° - \gamma \Rightarrow \bar{\theta} = \frac{90°}{180° - \gamma}\theta \tag{62}$$

$$\theta > 180° - \gamma \Rightarrow \bar{\theta} = \frac{90°}{\gamma}(\theta - (180° - \gamma)) + 90° \tag{63}$$

Simplifying this equation yields

$$\theta > 180° - \gamma \Rightarrow \bar{\theta} = 180° + \frac{90°}{\gamma}(\theta - 180°) \tag{64}$$

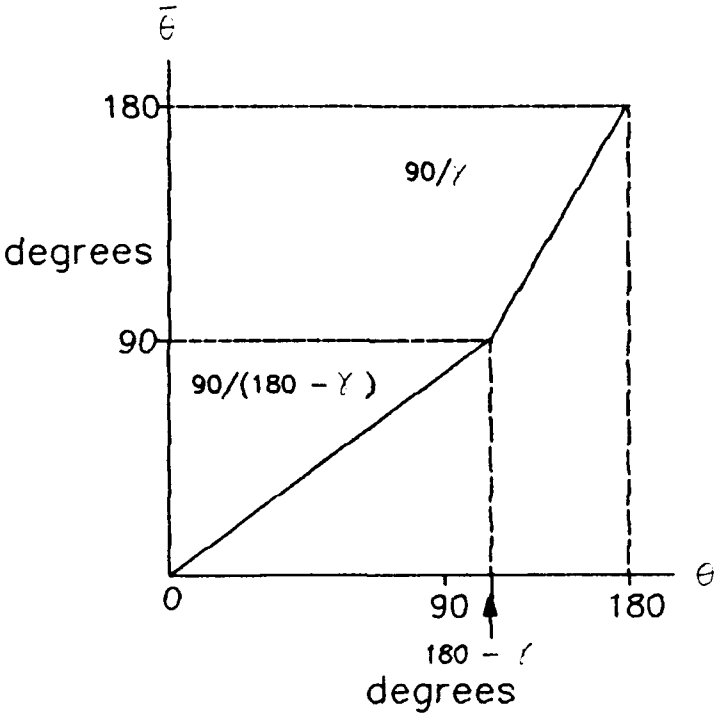

Figure 5 Slopes of the transformation from θ to $\bar{\theta}$

4.2.2. Cartesian Coordinates.

The next step is to convert these equations to Cartesian coordinates. For this transformation, the radius between coordinates is assumed constant, i.e. rotate the damping ratio line to the imaginary axis keeping the distance from the origin constant. The equations to convert to Cartesian coordinates are

$$x = r\cos\theta \qquad y = r\sin\theta$$

$$r = \sqrt{x^2 + y^2} \qquad \theta = \tan^{-1}\left(\frac{y}{x}\right) \tag{65}$$

Note that the equation for θ above will introduce an ambiguity.

Case 1: $\theta \leq 180° - \gamma$

$$\bar{x} = r\cos\bar{\theta} = \sqrt{x^2 + y^2}\cos\left[\left(\frac{90°}{180° - \gamma}\right)\tan^{-1}\left(\frac{y}{x}\right)\right] \tag{66}$$

$$\bar{y} = r\sin\bar{\theta} = \sqrt{x^2 + y^2}\sin\left[\left(\frac{90°}{180° - \gamma}\right)\tan^{-1}\left(\frac{y}{x}\right)\right] \tag{67}$$

Case 2: $\theta > 180° - \gamma$

$$\bar{x} = r\cos\bar{\theta} = -\sqrt{x^2 + y^2}\cos\left[\left(\frac{90°}{\gamma}\right)\left(\tan^{-1}\left(\frac{y}{x}\right) - 180°\right)\right] \tag{68}$$

$$\bar{y} = r\sin\bar{\theta} = -\sqrt{x^2 + y^2}\sin\left[\left(\frac{90°}{\gamma}\right)\left(\tan^{-1}\left(\frac{y}{x}\right) - 180°\right)\right] \tag{69}$$

The equations for the ζ rotation are considerably more complicated than for the α shift. Not only does each equation have complicated terms, but there are different equations for different parts of the plane. Some type of 'if/then' programming logic would be required to implement them. Also, the $\tan^{-1}$ term in each equation will cause a problem. Mathematically, two solutions are possible, but only one is correct.

4.3. Combined α Shift and ζ Rotation

The next logical step would be to combine an α shift and a ζ rotation. The easiest method is to first rotate the imaginary axis to some angle γ and then shift the entire plane by α. Figure 6 shows these transformations. For this section, the first transformation is designated by a bar ($\bar{y}$) and the second transformation is designated by a hat ($\hat{y}$).

The equations for this are very similar to the ones from Section 4.2.2 The new equations are

$$\hat{y} = \bar{y} \qquad \hat{x} = \bar{x} + \alpha \tag{70}$$

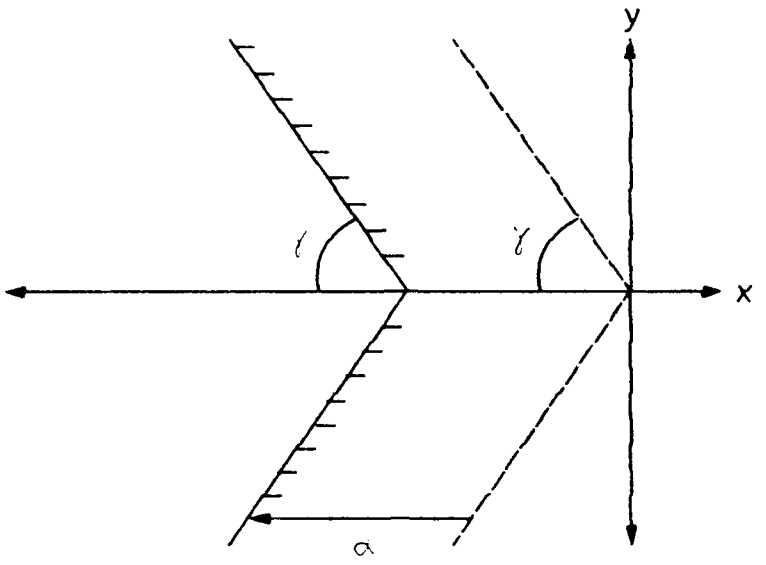

Figure 6 Combined α shift and ζ rotation

Substituting the results from Section 4.2.2 yields the following equations:

For $\theta \leq 180° - \gamma$:

$$\hat{x} = \sqrt{x^2 + y^2}\cos\left[\left(\frac{90°}{180° - \gamma}\right)\tan^{-1}\left(\frac{y}{x}\right)\right] + \alpha \tag{71}$$

$$\hat{y} = \sqrt{x^2 + y^2}\sin\left[\left(\frac{90°}{180° - \gamma}\right)\tan^{-1}\left(\frac{y}{x}\right)\right] \tag{72}$$

For $\theta > 180° - \gamma$:

$$\hat{x} = -\sqrt{x^2+y^2}\cos\left[\left(\frac{90°}{\gamma}\right)\left(\tan^{-1}\left(\frac{y}{x}\right) - 180°\right)\right] + \alpha \tag{73}$$

$$\hat{y} = -\sqrt{x^2+y^2}\sin\left[\left(\frac{90°}{\gamma}\right)\left(\tan^{-1}\left(\frac{y}{x}\right) - 180°\right)\right] \tag{74}$$

These equations are not much more complicated than the ζ rotation. The equations for the ζ rotation and the α shift can be combined directly with no additional effort. The next section will show how the transformations affect a vertical line at -7.

4.4. Effects of the Transformation on a Vertical Line

We will begin with a vertical line at x = -7 and first perform just a ζ rotation, and then both a ζ rotation and an α shift. Figure 7 shows the vertical line at -7 and also the new y axis after a ζ rotation of 45°. The hatched line shows the boundary of the new region that will be considered stable.

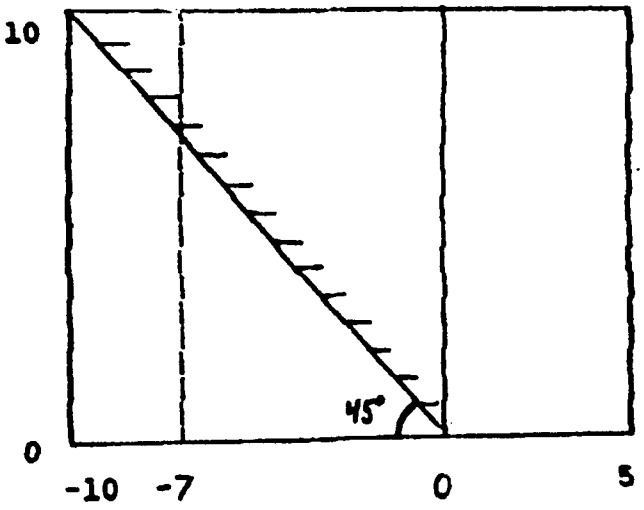

Figure 7 Line before coordinate transformation

Figure 8 shows the line after a ζ rotation of 45°. Note how it begins at x = -7 and crosses the new x = 0 line just below y = 10. From Figure 7 the distance to the point where the vertical line crosses the 45° line is 9.89. Since r is held constant over the transformation this is exactly what was expected.

Figure 9 shows the line after a ζ rotation of 45° and an α shift of 5. It is simply Figure 8 shifted by 5.

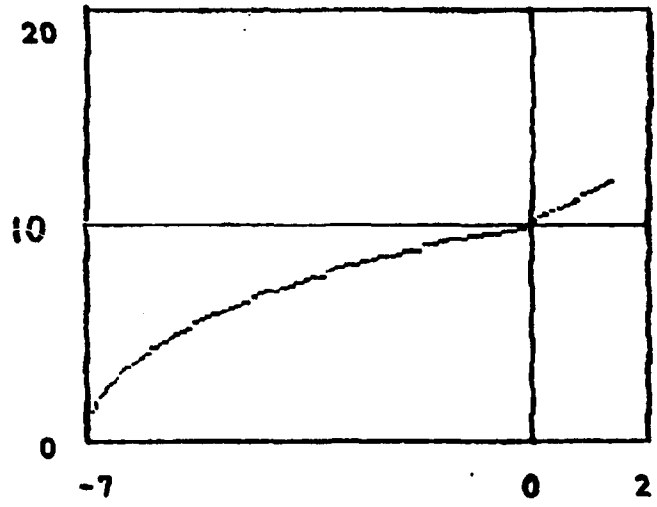

Figure 8 Line after ζ rotation

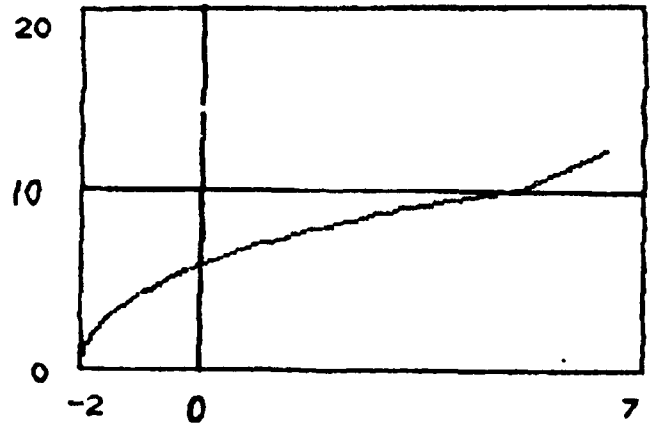

Figure 9 Line after combined transformation

This chapter derived the equations for transforming the complex plane. The next chapter will put the α shift into state space equations.

5. State Space Equations for the α Shift

In order to be used in the H_2 and H_∞ optimization equations from Chapter 2, the equations derived in the previous chapter must be converted from Cartesian coordinates to state space equations. The easiest way to do this is to first convert them to the Laplace Domain s-plane and then to state space. For the α shift this is relatively easy. The y (imaginary) axis is moved to the left by α and the x (real) axis is not changed. Looking at this in terms of the s-plane,

$$s' = s + \alpha \tag{75}$$

or

$$s = s' - \alpha \tag{76}$$

where s' denotes the transformed s-plane.

The transfer function matrix equation relating the state space equations to the Laplace domain is

$$G(s) = C(sI - A)^{-1}B \tag{77}$$

Substituting $s = s' - \alpha$ into this equation yields

$$G(s') = C((s' - \alpha)I - A)^{-1}B \tag{78}$$

$$= C(s'I - \alpha I - A)^{-1}B \tag{79}$$

Let

$$A' = \alpha I + A = A + \alpha I \tag{80}$$

Substituting this into (77) yields

$$G(s') = C(s'I - A')^{-1}B \tag{81}$$

This is the standard transfer function matrix form again. These results appear rather simple, but are very powerful. To α shift the state space equations, all that is required is to add αI to the A matrix. The new state space equations are

$$\dot{x} = A'x + Bu \tag{82}$$

$$y = Cx \tag{83}$$

where

$$A' = A + \alpha I \tag{84}$$

As described in Section 3.1, these equations were first derived by Anderson and Moore in 1969 [3]. They worked completely in the time domain using $e^{\alpha t}$ as a weighting factor on the performance index. Their derivation and what is presented here can be reconciled by the Laplace Transform identity

$$e^{\alpha t}F(t) \Rightarrow f(s-\alpha) \tag{85}$$

6. Example Problem 1

6.1. Block Diagrams and Generalized State Space Equations

The first example problem uses the system configuration shown in Figure 10. The outputs of interest are e_1 and e_2. The output e_1 weighted by W_s provides control over the shape of the sensitivity function and the output e_2 weighted by W_u provides control over the amount of control power the compensator will use.

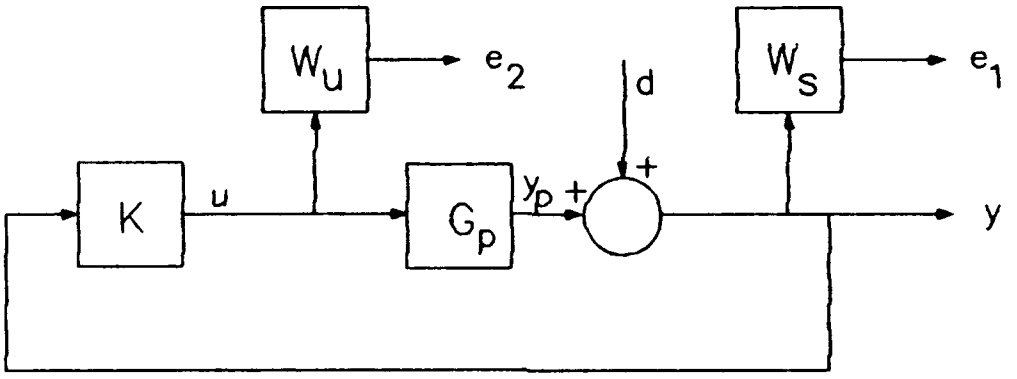

Figure 10 Block diagram for Example 1 with the weighting factors

The first step is to put the system into standard form. Standard form requires state space equation of the form

$$\dot{x} = Ax + B_d d + B_u u \tag{86}$$

$$e = C_e x + D_{ed} d + D_{eu} u \tag{87}$$

$$y = C_y + D_{yd} d + D_{yu} u \tag{88}$$

where the elements of the above equations must be found by manipulating the block diagram in Figure 10.

From Figure 10

$$\dot{x} = A_p x + B_p u \tag{89}$$

$$y_p = C_p x + D_p u = C_p x \tag{90}$$

$$y = d + y_p = d + C_p x \tag{91}$$

where G is assumed to be strictly proper.

The state space equations for the weighting factor W_e are:

$$\dot{x}_e = A_e x_e + B_e u_e = A_e x_e + B_e (d + C_p x) \tag{92}$$

$$e_1 = C_s x_s + D_s u_s = C_s x_s \tag{93}$$

For the Doyle/Glover parameterization given in Chapter 2, D_{ed} must be equal to 0. To insure this, we require that the weighting factor W_s be strictly proper, i.e. $D_s = 0$. The reason for this can be seen from Figure 10. If W_s had a D_s term, then the disturbance would have an open path to the output e_1 and D_{ed} would not equal 0.

In this example we will restrict the weighting W_u to be purely a gain, i.e. only a D_u term, but in general the state space equations for this block are

$$\dot{x}_u = A_u x_u + B_u u \tag{94}$$

$$e_2 = C_u x_u + D_u u \tag{95}$$

For the Doyle/Glover parameterization, $D_{eu}^T D_{eu}$ must be similar to I; that is, it must be full rank. In practice, this means that each element in u must go to one of the controlled outputs directly. To insure this, the W_u weighting factor must have a D_u term. Again looking at the block diagram in Figure 10, the reason for this is obvious. Since G and W_s are strictly proper, e_1 does not pick up u,

therefore u must pass through W_u by way of a D_u term.

Putting this in matrix form and dropping the W_u state equations, the system becomes

$$\begin{pmatrix}\dot{x}\\ \dot{x}_s\end{pmatrix}=\begin{pmatrix}A_p & 0\\ B_sC_p & A_s\end{pmatrix}\begin{pmatrix}x\\ x_s\end{pmatrix}+\begin{pmatrix}0\\ B_s\end{pmatrix}d+\begin{pmatrix}B_p\\ 0\end{pmatrix}u \tag{96}$$

$$\begin{pmatrix}e_1\\ e_2\end{pmatrix}=\begin{pmatrix}0 & C_s\\ 0 & 0\end{pmatrix}\begin{pmatrix}x\\ x_s\end{pmatrix}+\begin{pmatrix}0\\ 0\end{pmatrix}d+\begin{pmatrix}0\\ D_u\end{pmatrix}u \tag{97}$$

$$y=(C_p \quad 0)\begin{pmatrix}x\\ x_s\end{pmatrix}+(I)d+(0)u \tag{98}$$

From this we get the following matrices for each of the variables in Equations (86) - (88):

$$A=\begin{pmatrix}A_p & 0\\ B_sC_p & A_s\end{pmatrix} \qquad B_d=\begin{pmatrix}0\\ B_s\end{pmatrix} \qquad B_u=\begin{pmatrix}B_p\\ 0\end{pmatrix}$$

$$C_s=\begin{pmatrix}0 & C_s\\ 0 & 0\end{pmatrix} \qquad D_{sd}=\begin{pmatrix}0\\ 0\end{pmatrix} \qquad D_{su}=\begin{pmatrix}0\\ D_u\end{pmatrix}$$

$$C_y=(C_p \quad 0) \qquad D_{yd}=(I) \qquad D_{yu}=(0) \tag{99}$$

6.2. Numerical Values for the System Used

The test plant used for this example was

$$G(s) = \frac{2(s+2)(s+4)}{(s+1)(s+3)(s+5)} \tag{100}$$

This transfer function was chosen to show the results of shifting the region considered to be stable across several open-loop poles and zeros. For example, an α shift of 1.5 would require a compensator designed for an unstable system in the s' plane and an α shift of 2.5 would require a compensator designed for an unstable and nonminimum phase system in the s' plane.

Converting this to state space equations gives

$$A_p = \begin{pmatrix} -1 & 0 & 0 \\ 1 & -8 & -3.8730 \\ 0 & 3.8730 & 0 \end{pmatrix} \qquad B_p = \begin{pmatrix} 1 \\ 0 \\ 0 \end{pmatrix}$$

$$C_p = (2 \quad -4 \quad -3.6148) \qquad D_p = (0) \tag{101}$$

The W_s weighting function used for this example was:

$$W_s = \frac{1000(s+1)}{(s+.001)(s+1000)} \tag{102}$$

Figure 11 shows a singular value plot of W_s. This is chosen to have a shape that is the inverse of the desired sensitivity. As can be seen in Figure 11, the W_s weighting rolls off at very high frequency - this is necessary due to the strictly proper requirement. The desired sensitivity does not look like the inverse of W_s here, but since these frequencies are well beyond the bandwidth of the system, this will not affect the design. Converting this to state space equations

$$A_s = \begin{pmatrix} -1000 & -1 \\ 1 & 0 \end{pmatrix} \qquad B_s = \begin{pmatrix} 1 \\ 0 \end{pmatrix}$$

$$C_s = (1000 \quad 1000) \qquad D_s = (0) \tag{103}$$

The W_u used was

$$D_u = 0.01 \tag{104}$$

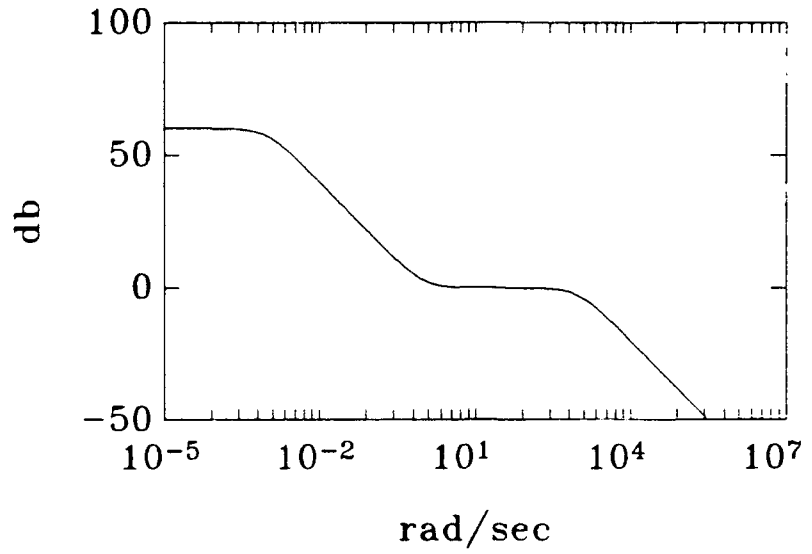

Figure 11 Singular Value plot of W',

Putting all this together into the standard format yields:

$$A = \begin{pmatrix} -1 & 0 & 0 & 0 & 0 \\ 1 & -8 & -3.873 & 0 & 0 \\ 0 & 3.873 & 0 & 0 & 0 \\ 2 & -4 & -3.6148 & -1000 & -1 \\ 0 & 0 & 0 & 1 & 0 \end{pmatrix}$$

$$B_d = \begin{pmatrix} 0 \\ 0 \\ 0 \\ 1 \\ 0 \end{pmatrix} \qquad B_u = \begin{pmatrix} 1 \\ 0 \\ 0 \\ 0 \\ 0 \end{pmatrix}$$

$$C_e = \begin{pmatrix} 0 & 0 & 0 & 1000 & 1000 \\ 0 & 0 & 0 & 0 & 0 \end{pmatrix}$$

$$C_y = (2 \quad -4 \quad -3.6148 \quad 0 \quad 0)$$

$$D_{ed} = \begin{pmatrix} 0 \\ 0 \end{pmatrix} \qquad D_{eu} = \begin{pmatrix} 0 \\ .01 \end{pmatrix}$$

$$D_{yd} = (1) \qquad D_{yu} = (0) \qquad (105)$$

The above equations are in standard form for designing H_2 and H_∞ controllers. To close the loop and evaluate the performance of the closed-loop system, a slightly different form is required.

6.3. Closing the Loop

The block diagram configuration used to close the loop is shown in Figure 12. This is still standard form. To get

this configuration the block diagram shown in Figure 11 must be modified to include an input r. This modification is shown in Figure 13.

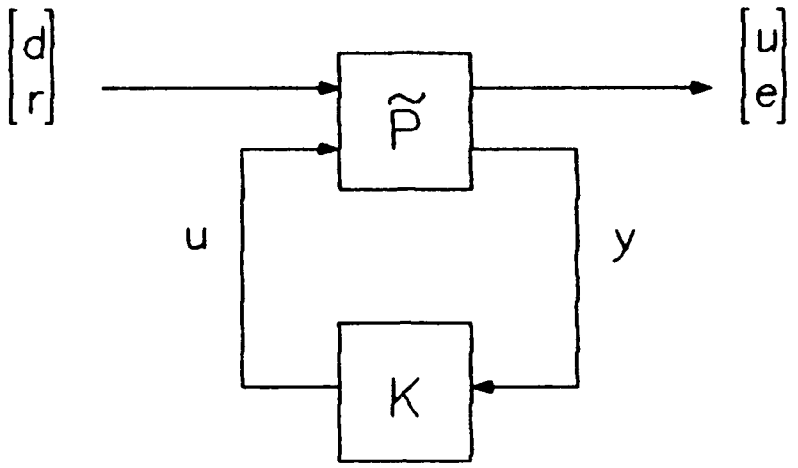

Figure 12 Block diagram for Example 1 in feedback format

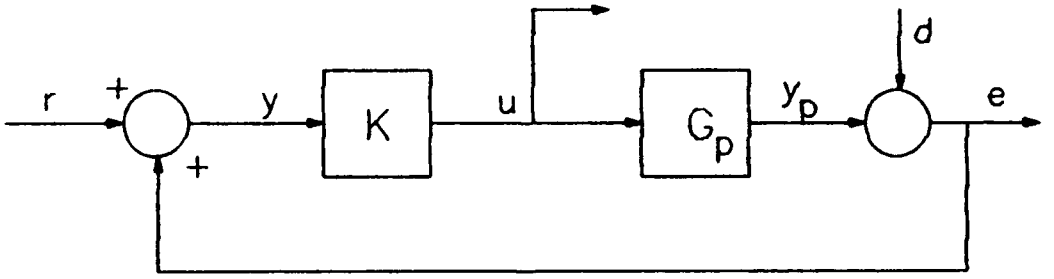

Figure 13 Block diagram for Example 1 with command input

The equations for this figure are

$$\dot{x} = A_p x + B_p u \tag{106}$$

$$y_p = C_p x \tag{107}$$

$$e = y_p + d = C_p x + d \tag{108}$$

$$y = r + e = r + C_p x + d \tag{109}$$

Putting these equations into matrix form yields

$$\dot{x} = A_p x + (0 \quad 0)\begin{pmatrix} d \\ r \end{pmatrix} + B_p u \tag{110}$$

$$\begin{pmatrix} u \\ e \end{pmatrix} = \begin{pmatrix} 0 \\ C_p \end{pmatrix} x + \begin{pmatrix} 0 & 0 \\ I & 0 \end{pmatrix}\begin{pmatrix} d \\ r \end{pmatrix} + \begin{pmatrix} I \\ 0 \end{pmatrix} u \tag{111}$$

$$y = C_p x + (I \quad I)\begin{pmatrix} d \\ r \end{pmatrix} \tag{112}$$

Putting the numbers for Example 1 into the above equations yields

$$A=\begin{pmatrix}-1 & 0 & 0\\ 1 & -8 & -3.873\\ 0 & 3.873 & 0\end{pmatrix} \qquad B_d=\begin{pmatrix}0 & 0\\ 0 & 0\\ 0 & 0\end{pmatrix} \qquad B_u=\begin{pmatrix}1\\ 0\\ 0\end{pmatrix}$$

$$C_z=\begin{pmatrix}0 & 0 & 0\\ 2 & -4 & -3.6148\end{pmatrix} \qquad D_{zd}=\begin{pmatrix}0 & 0\\ 1 & 0\end{pmatrix} \qquad D_{zu}=\begin{pmatrix}1\\ 0\end{pmatrix}$$

$$C_y=(2 \quad -4 \quad -3.6148) \qquad D_{yd}=(1 \quad 1) \qquad D_{yu}=0 \qquad (113)$$

6.4. Mechanics of the α Shift

To accomplish the α shift, only the A_p portion of the A matrix (see Equation 99) is changed. It is important that αI is added only to A_p, and not to the portion of the A matrix that contains the weighting functions. The compensator K is then designed using standard H_2 and H_∞ optimization methods. Once the compensator is designed it must be reverse shifted back to the standard s-plane. This is accomplished by subtracting αI from A_k, where A_k is the A matrix of the compensator.

6.5. Results for H_2 Optimization

The next step is to perform H_2 and H_∞ compensator design on the matrix equations derived in Section 6.2. This will yield a compensator that minimizes the 2 or ∞ norm of the weighted closed-loop system. The loop is then closed around the compensator using the block diagram and the matrix equations derived in Section 6.3. For the sake of brevity, only selected α shifts for the H_2 optimization design method are presented here. Table 2 at the end of Section 6.5 compares the closed-loop poles and transmission zeros for α = 0, 1.5 and 2.5. The shifted plant for α = 0 is stable and minimum phase, for α = 1.5 is unstable and for α = 2.5 is unstable and nonminimum phase.

6.5.1. α=0 (Original Plant).

This section shows how the closed-loop system performs with no α shift; i.e. standard H_2 optimization. Figure 14 shows the sensitivity for the system. It starts at -60 db, breaks upward at w = 0.001 and levels off at 0 db. This is a very good sensitivity and is exactly what was asked for by the weighting function W_s.

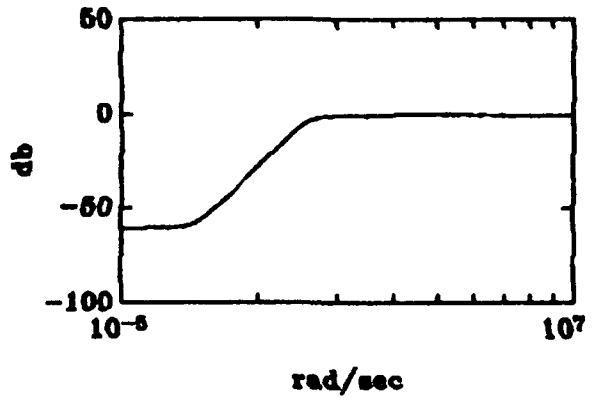

Figure 14 Sensitivity for Example 1 with no α shift

Figure 15 shows the amount of control energy required. Note the dip around 1 rad/sec and the peak just below 20 db.

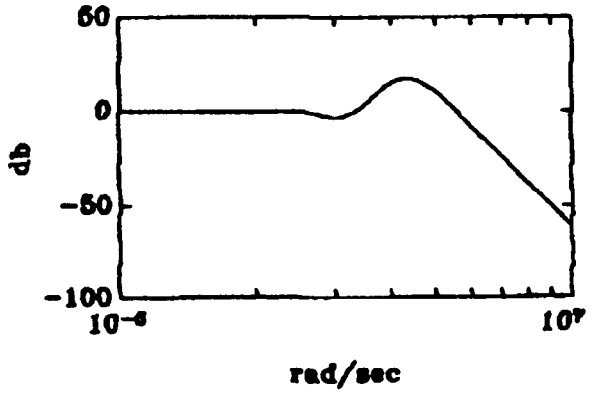

Figure 15 Control usage with no α shift

Figure 16 shows the time response of the system due to a unit step command input (e to r). Note the excellent command following and the relatively slow rise time.

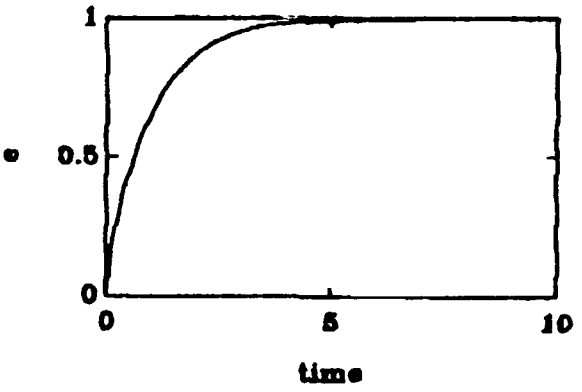

Figure 16 Response to a unit step command input with no α shift

As can be seen from the above figures, this was a very simple case. The plant was already stable and minimum phase. The sensitivity has a good shape and the time response tracked to the desired final value of 1 perfectly.

6.5.2. $\alpha = 1.5$ (Unstable).

This case is a little more difficult. Shifting all of the poles left of -1.5 will require "stabilizing" the pole at -1 from the plant. Figure 17 shows the sensitivity.

Note how much the low frequency end has changed. For the unshifted case it started at -60 db (as it should because of the gain of 1000 in W_s), but for the shift of 1.5 it starts at -12 db.

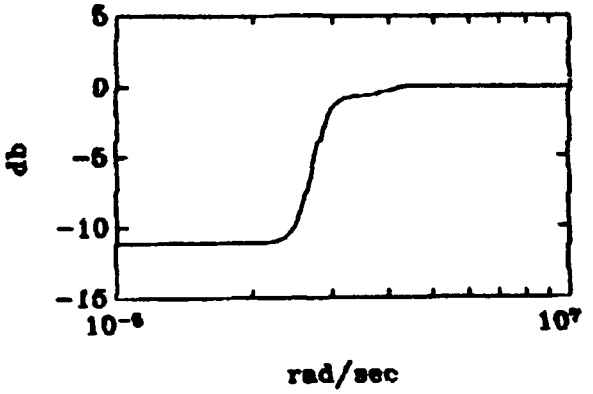

Figure 17 Sensitivity for Example 1 with 1.5 α shift

Figure 18 shows the control power required. Note the slight drop at low frequencies and the increase around 1 rad/sec.

Figure 19 shows the time response to a unit step command step input (e to d). The system responds much faster, but the final value is significantly degraded to 0.7 rather than 1.

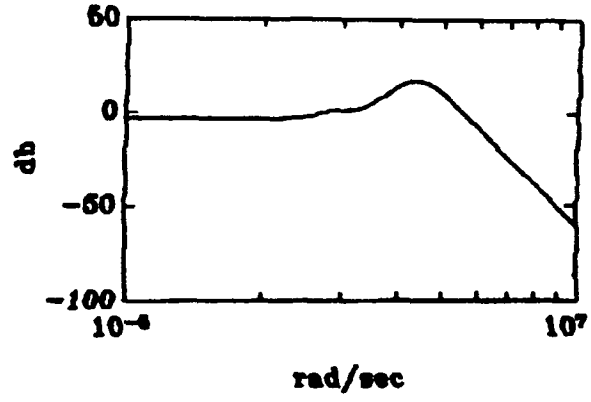

Figure 18 Control usage with 1.5 α shift

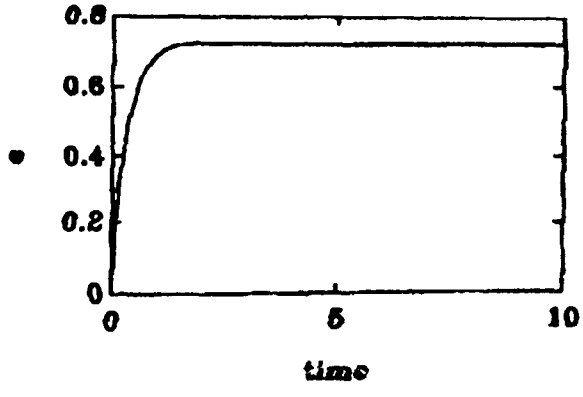

Figure 19 Response to a unit step command input with 1.5 α shift

6.5.3. $\alpha = 2.5$ (Unstable and Nonminimum Phase).

Shifting the region considered to be stable left of -2.5 makes the problem considerably more difficult. Now not only

must the compensator move the pole at -1, but also must avoid having the zero at -2 pull a pole right of -2.5. Figure 20 shows the sensitivity. Again note the starting point of -12 db. As can be seen, increasing the shift from 1.5 to 2.5 does not affect the sensitivity very much.

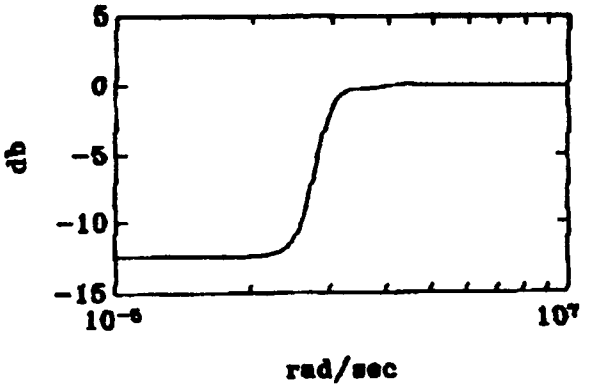

Figure 20 Sensitivity for Example 1 with 2.5 α shift

Figure 21 shows the control power required. Note the rather large increase around 1 rad/sec.

Figure 22 shows the time response to a unit step command input. Note the greatly increased speed of response, the final value of 1.2, and for the first time an overshoot.

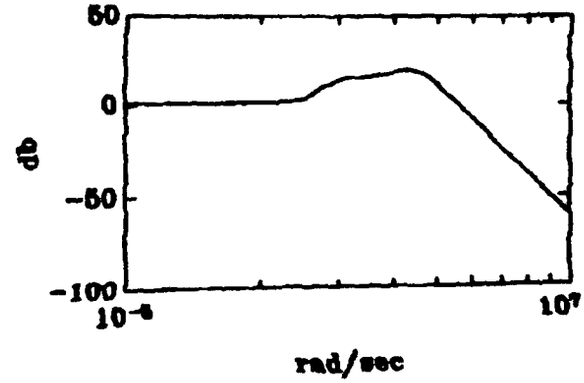

Figure 21 Control usage with 2.5 α shift

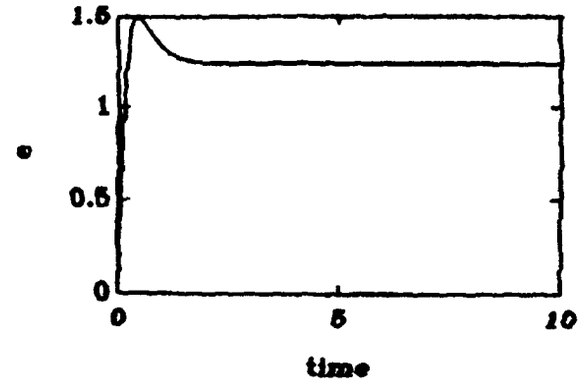

Figure 22 Time response to a unit step command input for Example 1 with a 2.5 α shift

6.5.4. Conclusions for H_2 Optimization.

Table 1 gives a summary of the results shown above, as well as for other α shifts. Note how the 2 norm, the

control usage, the control rate, and the steady state error increase as α is increased. Also note how the speed increases up to a certain point and then slows down again. Obviously, only the smaller α shifts are reasonable for any kind of design.

Table 1 Summary of H_2 optimization results

	α shift				
	0	1.5	2.5	3.5	5.5
2 norm	246.7	249.4	283.5	501.5	11514
Control usage	5.8	6.0	7.6	22	610
Control rate	3000	3000	4000	1100	61000
Rejection error	0%	30%	30%	80%	200%
Rejection time	2.5	1	0.5	1	1
Tracking error	0%	30%	30%	80%	200%
Tracking time	2.5	1	0.5	1	1

Table 2 shows the closed-loop poles and zeros. As can be seen, the α shift does exactly what it is designed to do; specifically, it moves all of the closed-loop poles left of $-\alpha$.

Table 2 Closed-loop poles and zeros for Example 1

$\alpha = 0$		$\alpha = 1.5$		$\alpha = 2.5$	
poles	zeros	poles	zeros	poles	zeros
-978.9	-11.78	-980.4	-24.16	-981.4	-380.2
-204.3	-5	-205.8	-5	-206.8	-5
-5	-5	-5	-5	-5	-5
-4	-3	-4	-3	-4	-3
-3	-3	-3	-3	-4	-2.662
-2	-1	-2.5	-1	-3.5	-1
-1	-1	-2		-3	
-1		-2		-3	

Another interesting result is the change in the 2 norm. For the unshifted case the 2 norm is 246.7. For an α shift of 1.5 the 2 norm has increased to 249.4 and for an α shift of 2.5 the 2 norm has increased to 283.5. Note that there is relatively little change as the shift crosses a pole, but a much larger increase as it crosses a zero. This is to be expected. Crossing a pole is the same as putting one more unstable pole in the plant. This is not a major problem for a minimum phase system. It is relatively easy to move poles around. Crossing a zero, however, is more of a problem.

This is the same as having one more nonminimum phase zero in the plant. The poles move to the zeros as gain is increased, so having a pole and a zero in the right half plane is a very tricky problem. The compensator must send a pole into the right half plane to split the unstable plant pole off the real axis and pull them both into the left half plane without allowing the zero to draw a pole to the right half plane.

The shift of the closed-loop poles shows up very clearly in the time response plots. As α is increased the time response get much faster. One problem is the degradation of the final value that the time response approaches. For good command following it should go to 1. One way to improve this would be to add a bank of integrators to the system. Another possible solution would be to experiment with the W_e weighting factor or to decrease the W_u parameter to allow the system to use more control power.

6.6. Results for H_∞ Optimization

The shape of the plots and the effects of the α shift are very similar to H_2 optimization for H_∞ optimization. The magnitude does change in the plots, but trends remain the same. The results are summarized in Table 3.

Example 1 showed the results of shifting across a pole and/or zero, and the trends and limits as α is increased. It also presented the mechanics of the method. The next example will test this method on a real design problem.

Table 3 Summary of H_∞ optimization results

	α shift				
	0	1.5	2.5	3.5	5.5
Gamma	0.855	0.856	6.009	13.44	268
Control usage	75	75	550	1200	25000
Control rate	75000	75000	$5.5*10^5$	$1.2*10^6$	$2.5*10^7$
Rejection error	0%	25%	100%	120%	200%
Rejection time	2.5	1	0.5	0.5	1
Tracking error	0%	25%	100%	120%	200%
Tracking time	2.5	1	0.5	0.5	1

7. Example Problem 2

7.1. Problem Statement

The previous example showed the mechanics of how the α shift works. This example applies it to a problem taken from [10:13-1]. The problem is to design a lateral attitude control system for a drone aircraft. The state space equations for this example are

$$\dot{x} = Ax + Bu \tag{114}$$

$$y = Cx + Du \tag{115}$$

where:

$$A = \begin{pmatrix} -0.08527 & -0.0001423 & -0.9994 & 0.04141 & 0 & 0.1862 \\ -46.86 & -2.757 & 0.3896 & 0 & -124.3 & 128.6 \\ -0.4248 & -0.06224 & -0.6714 & 0 & -8.792 & -20.46 \\ 0 & 1 & 0.0523 & 0 & 0 & 0 \\ 0 & 0 & 0 & 0 & -20 & 0 \\ 0 & 0 & 0 & 0 & 0 & -20 \end{pmatrix} \tag{116}$$

$$B = \begin{pmatrix} 0 & 0 \\ 0 & 0 \\ 0 & 0 \\ 0 & 0 \\ 20 & 0 \\ 0 & 20 \end{pmatrix} \tag{117}$$

$$C = \begin{pmatrix} 1 & 0 & 0 & 0 & 0 & 0 \\ 0 & 0 & 0 & 1 & 0 & 0 \end{pmatrix} \tag{118}$$

$$D = \begin{pmatrix} 0 & 0 \\ 0 & 0 \end{pmatrix} \tag{119}$$

$$x = [\beta \quad \phi \quad \dot{\psi} \quad \phi \quad \delta_e \quad \delta_r]^T \tag{120}$$

$$u = [\delta_{e_c} \quad \delta_{r_c}]^T \tag{121}$$

The states x are sideslip angle, roll rate, yaw rate, roll angle, elevon surface deflection, and rudder surface deflection. The inputs u are elevon servo command and rudder servo command. The open-loop plant has one zero at -158.15. The open-loop poles are shown in Table 4. Obviously, the compensator must stabilize the unstable dutch roll mode. The following figures and tables show that H_2 optimization simply pulls that complex pair to its mirror

image on the left side of the imaginary axis and then adds complex zeros very close by to nearly cancel the effects of the lightly damped complex poles.

Table 4 Open-loop poles

Dutch Roll (unstable)	0.1884 ± 1.0511 i
Spiral Mode	-0.0360
Roll Convergence	-3.2503
Elevon Actuator	-20.0
Rudder Actuator	-20.0

7.2. H_2 Optimization Setup and Equations

Figure 23 shows the block diagram for designing the compensator. Note the additional output (e_2) which is simply the output from the plant. The output e_2 is required for this problem because we want to control the complimentary sensitivity as well as the sensitivity. The complimentary sensitivity is the transfer function from d to e_2. The other two outputs, e_1 and e_3, are the same ones as used in the previous example. e_3 is the control input u weighted by an identity matrix multiplied by some constant ρ. The parameter ρ is the weighting penalty on control

usage. As ρ is lowered the system is allowed to use more control power. For this problem ρ was chosen to be 0.05. For $\rho = 0.05$ the maximum deflections and rates of the control surfaces (rudder and elevon) are within the range allowed on a real aircraft.

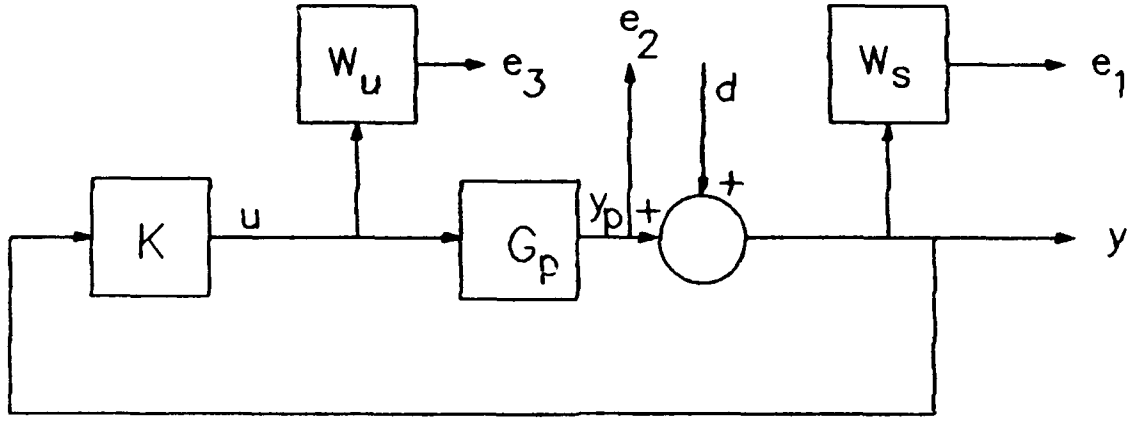

Figure 23 Block diagram for design on Example 2

e_1 is the output y weighted by some strictly proper transfer function matrix W_s. W_s is chosen so that, for low frequencies, the sensitivity will be its mirror image across the 0 db line. In Example 2, W_s is a 2x2 diagonal transfer function matrix. The 1,1 and 2,2 elements are the same and equal to

$$W_{su} = \frac{1000(s+1)}{(s+.001)(s+1000)} \qquad i = 1,2 \tag{122}$$

This is the same as the W_s from Example 1. In the following equations the subscript p refers to the plant (G) and the subscript s refers to the W_s weighting function.

The equations we are working towards are

$$\dot{x} = Ax + B_d d + B_u u \tag{123}$$

$$e = C_e x + D_{ed} d + D_{eu} u \tag{124}$$

$$y = C_y + D_{yd} d + D_{yu} u \tag{125}$$

Following the same procedure as in Example 1 the final state space equations become

$$\begin{pmatrix} \dot{x}_p \\ \dot{x}_s \end{pmatrix} = \begin{pmatrix} A_p & 0 \\ B_s C_p & A_s \end{pmatrix} \begin{pmatrix} x_p \\ x_s \end{pmatrix} + \begin{pmatrix} 0 \\ B_s \end{pmatrix} d + \begin{pmatrix} B_p \\ 0 \end{pmatrix} u \tag{126}$$

$$\begin{pmatrix} e_1 \\ e_2 \\ e_3 \end{pmatrix} = \begin{pmatrix} 0 & C_s \\ C_p & 0 \\ 0 & 0 \end{pmatrix} \begin{pmatrix} x_p \\ x_s \end{pmatrix} + \begin{pmatrix} 0 \\ 0 \\ 0 \end{pmatrix} d + \begin{pmatrix} 0 \\ 0 \\ \rho \end{pmatrix} u \tag{127}$$

$$y = (C_p \quad 0)\begin{pmatrix} x_p \\ x_s \end{pmatrix} + (I)d + (0)u \tag{128}$$

The above setup is used only to find the compensator K. The closed-loop format is the same as from Example 1. Figure 24 shows the standard MIMO feedback configuration. As in Example 1, the block diagram in Figure 24 must first be modified to include a command input r. The weighting factors W_u and W_s must also be removed. They are included only as design parameters to find the desired compensator. Figure 25 shows the modified block diagram used to find Figure 24.

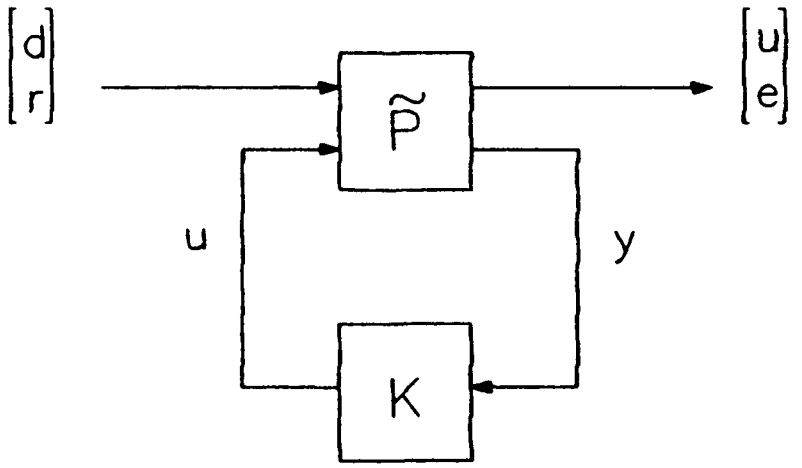

Figure 24 Block diagram for Example 2 in feedback format

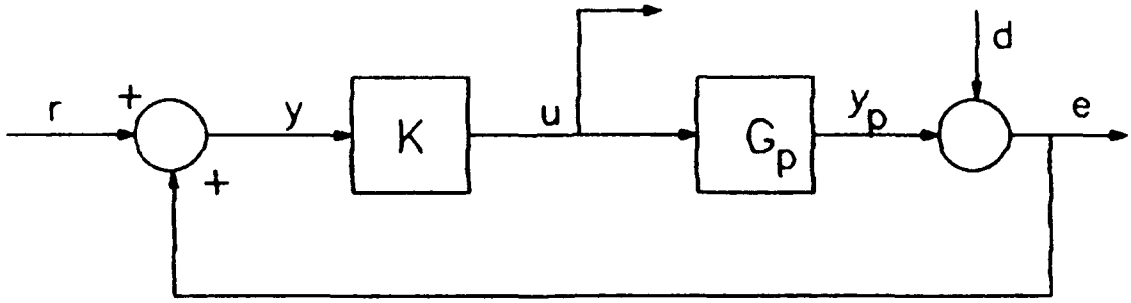

Figure 25 Block diagram for Example 2 with command input

The state space equations for this form are

$$\dot{x} = A_p x + (0 \quad 0)\begin{pmatrix} d \\ r \end{pmatrix} + B_p u \tag{129}$$

$$\begin{pmatrix} u \\ e \end{pmatrix} = \begin{pmatrix} 0 \\ C_p \end{pmatrix} x + \begin{pmatrix} 0 & 0 \\ I & 0 \end{pmatrix}\begin{pmatrix} d \\ r \end{pmatrix} + \begin{pmatrix} I \\ 0 \end{pmatrix} u \tag{130}$$

$$y = C_p x + (I \quad I)\begin{pmatrix} d \\ r \end{pmatrix} \tag{131}$$

These equations will be used to test the response of the system to both a step disturbance and a step command input.

7.3. H_2 Optimization with no α Shift

For ρ = 0.05 and no α shift the 2 norm is 12.12. The sensitivity is shown in Figure 26. This sensitivity is exactly what was asked for by the weighting function W_s.

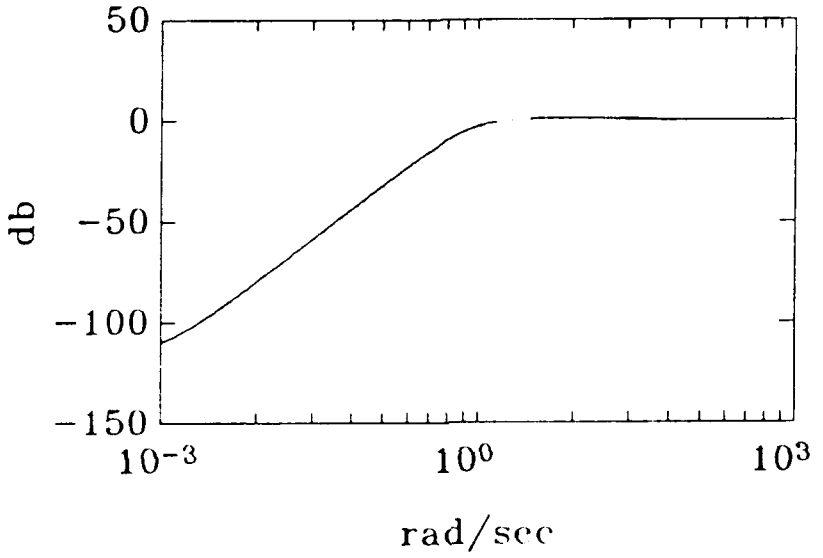

Figure 26 Sensitivity for Example 2 with no α shift

Figure 27 shows the control surface deflection in degrees required for a unit step β (sideslip angle) command. The maximum deflection is slightly more than -0.6 degrees and the maximum rate is less than 15 degrees per second.

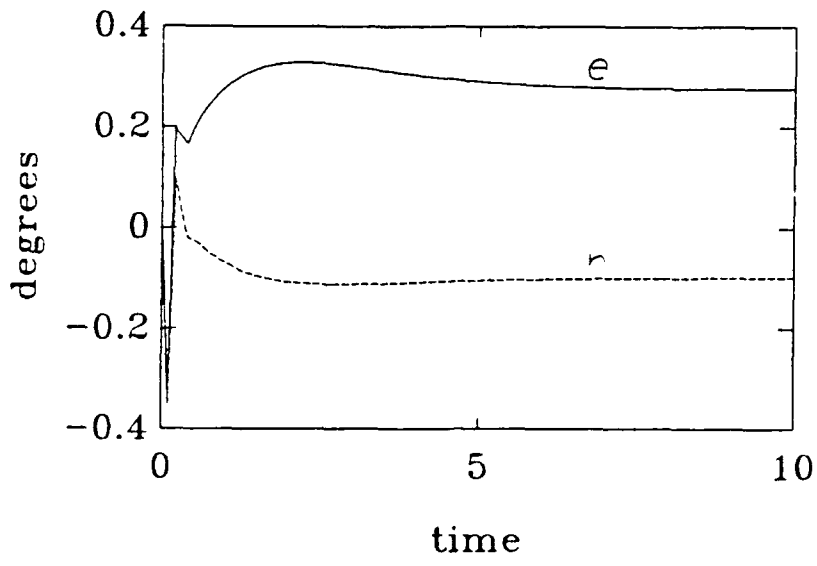

Figure 27 Control power required for a unit step β command

Figure 28 shows the control surface deflection in degrees required for a unit step ϕ (roll angle) command. The maximum deflection is less than 0.4 degrees and the maximum rate is less than 20 degrees per second.

Figure 29 shows how the system responds to a unit step sideslip angle disturbance. In about 10 seconds the disturbance is completely rejected. The sideslip returns to 0 fairly quickly with minimal oscillation.

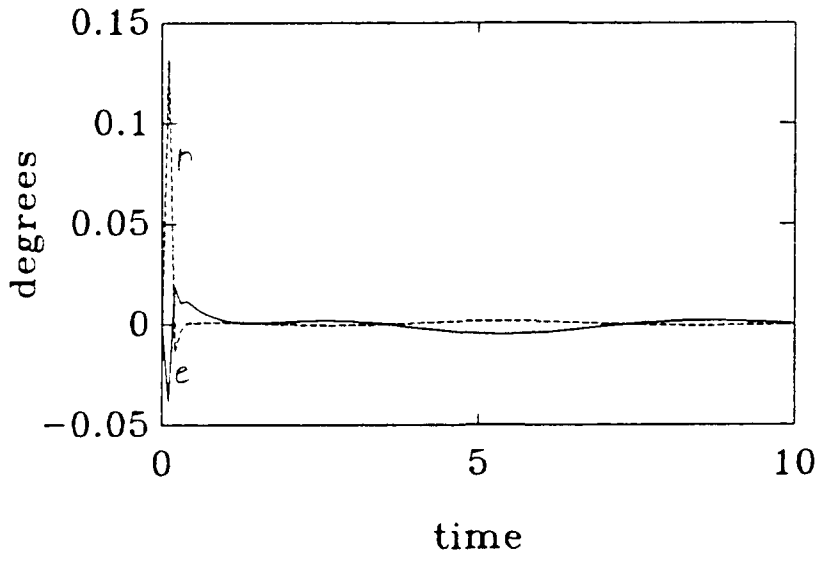

Figure 28 Control power required for a unit step ϕ command

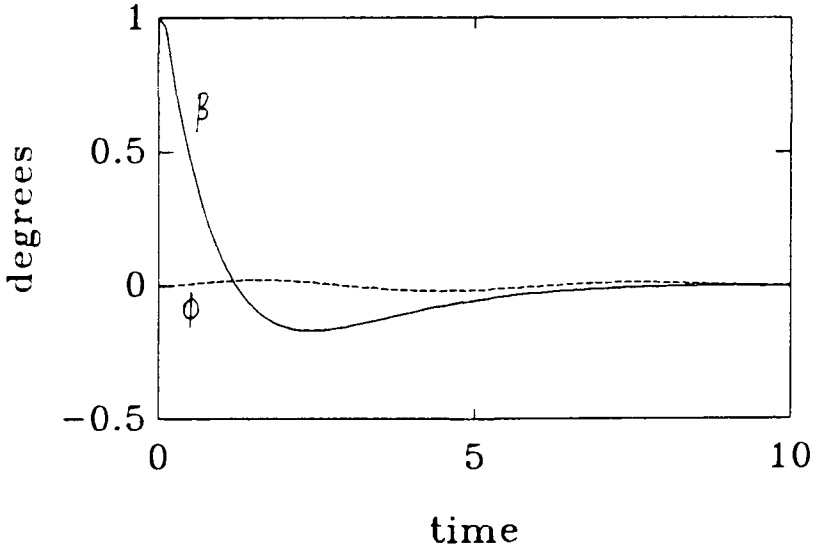

Figure 29 Rejecting a unit step β disturbance

Figure 30 shows how the system responds to a unit step roll angle disturbance. Note the time scale on this figure. The oscillations extend beyond 20 seconds.

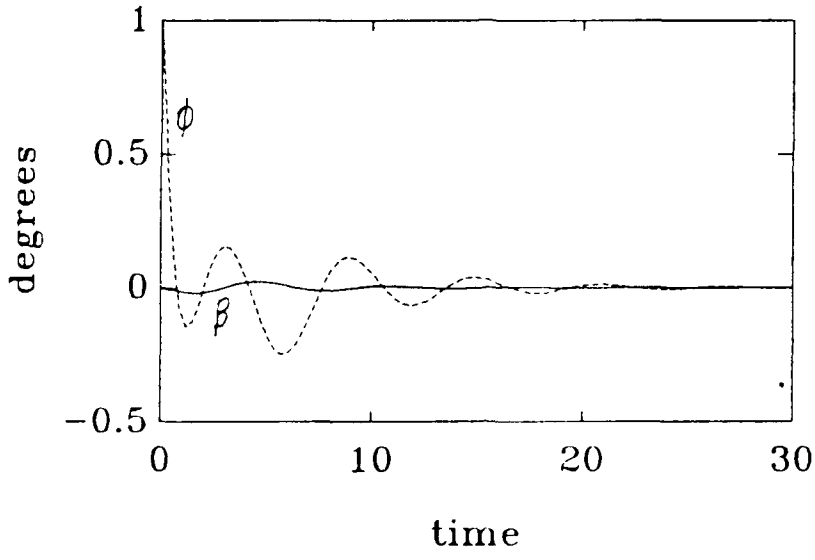

Figure 30 Rejecting a unit step ϕ disturbance

Figure 31 gives the command response of the system to a unit step β command. Within 5 seconds the system goes exactly to the desired value.

Figure 32 gives the command response of the system to a unit step ϕ command. Note the time scale again. The response still has oscillations at 20 seconds.

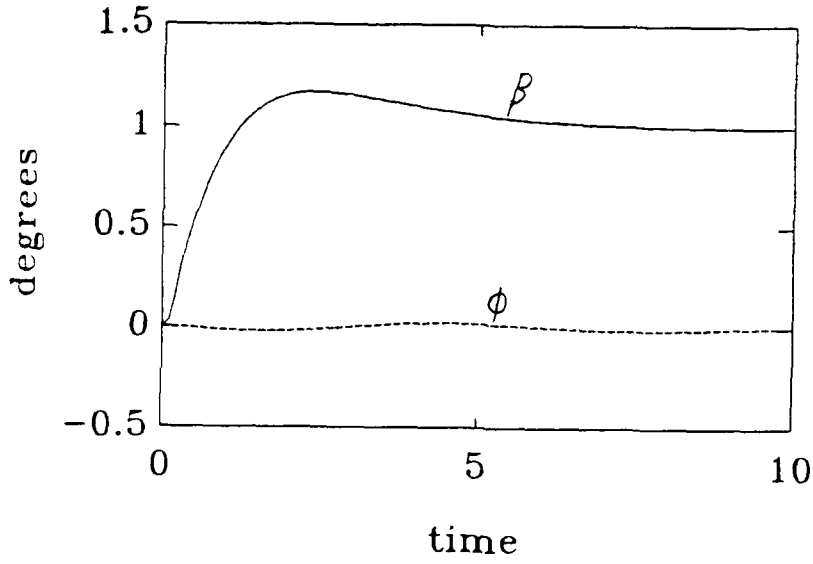

Figure 31 System response to a unit step β command input

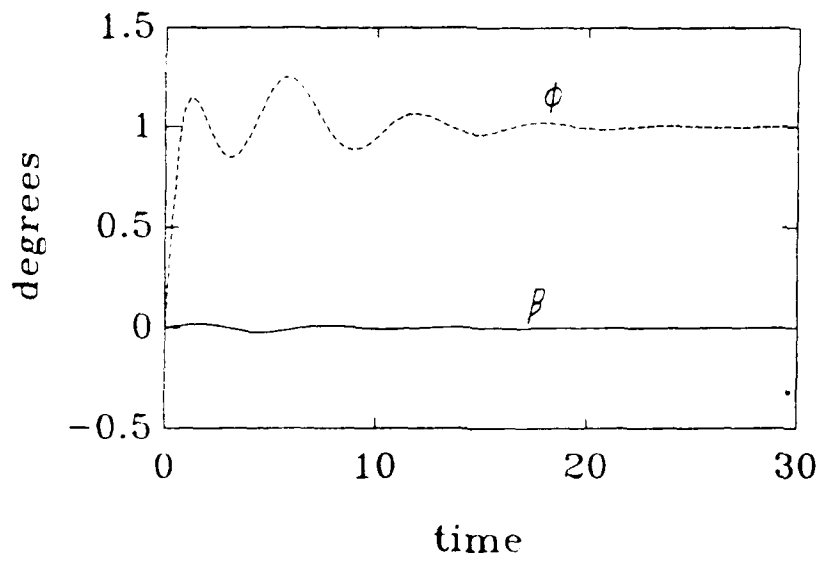

Figure 32 System response to a unit step ϕ command input

Overall, the system performance is not too bad. It will completely reject any disturbance and tracks command inputs perfectly in the steady state. The control deflections and rates are well within the capabilities of the actuators. The β disturbance rejection and command following are fairly quick and have little oscillation. The only problem is in the ϕ disturbance rejection and command following. The oscillations do not damp out for at least 20 seconds. Table 5 shows the low frequency closed-loop poles and zeros for the system. There are an additional 12 poles and 8 zeros with a magnitude greater than 10. They are not shown here because they have very little effect on the response.

Figure 33 shows the location of the poles and zeros with a magnitude less than 10 in the s-plane.

The open-loop poles at $0.18842 \pm 1.0511i$ have been moved to their mirror image location in the left half plane. The zero at $-0.057927 \pm 0.90067i$ is close enough to make the residue from the poles fairly small, but the poles have such poor damping that they cause the ringing effect in Figures 30 and 32.

Table 5 Closed-loop poles and zeros

poles	zeros
-0.035987	0.18842 ± 1.0511 i
-0.77686 ± 0.32181 i	-0.035987
-0.77689 ± 0.32180 i	-0.035987
-0.18842 ± 1.0511 i	-0.057927 ± 0.90067 i
-3.2503	-0.41344
	-0.43689
	-3.2503
	-3.2503

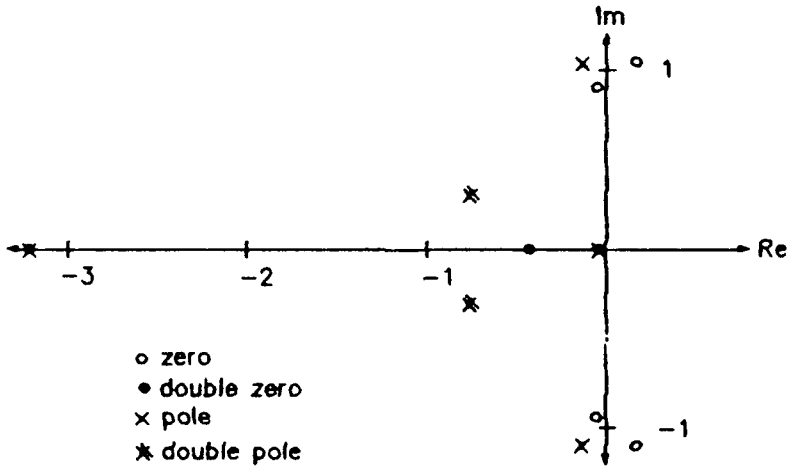

Figure 33 Poles and zeros for the unshifted case

The next section will show how an α shift of 0.3 changes the damping on those poles, and therefore the time response. As will be seen, the cost of the increased damping is decreased performance elsewhere.

7.4. H_2 Optimization with an α Shift of 0.3

The mechanics of the α shift are the same as for Example 1. Only the A_p portion of the A matrix is shifted, and A_k must be reverse shifted. An α shift of 0.3 seemed to give the best trade-off between increased damping and decreased performance. This moves the imaginary axis to -0.3 and the unstable poles at 0.18842 $\pm$ 1.0511i are moved to their mirror image across the new imaginary axis. Their closed-loop position is -0.78842 $\pm$ 1.0511i. Table 6 shows a summary of the results of an α shift from 0 to 0.9. For ρ = 0.05 and an α shift of 0.3 the 2 norm is 17.52. The 2 norm for the unshifted case was 12.12. As should be expected, the 2 norm has increased. The compensator is required to do more than before, and it will not be able to get to the same minimum 2 norm.

Table 6 Summary of H_2 optimization results

	α shift				
	0	0.2	0.3	0.4	0.9
2 norm	12.12	15.47	17.52	19.71	32.14
β dist. error (%)	0	5	8	11	30
β dist. time (sec)	8	4	4	3	2
ϕ dist. error (%)	0	0	0	0	0
ϕ dist. time (sec)	25	12	7.5	6	3
β track error (%)	0	5	8	11	30
β track time (sec)	8	4	4	3	2
ϕ track error (%)	0	0	0	0	0
ϕ track time (sec)	25	12	7.5	6	3

Figure 34 shows the sensitivity. Note the changes at low frequency. Before we had both channels beginning below -100 db and going smoothly to zero db at 1 rad/sec. For the shifted case one channel begins just below -20 db and neither of them are exactly what we wanted.

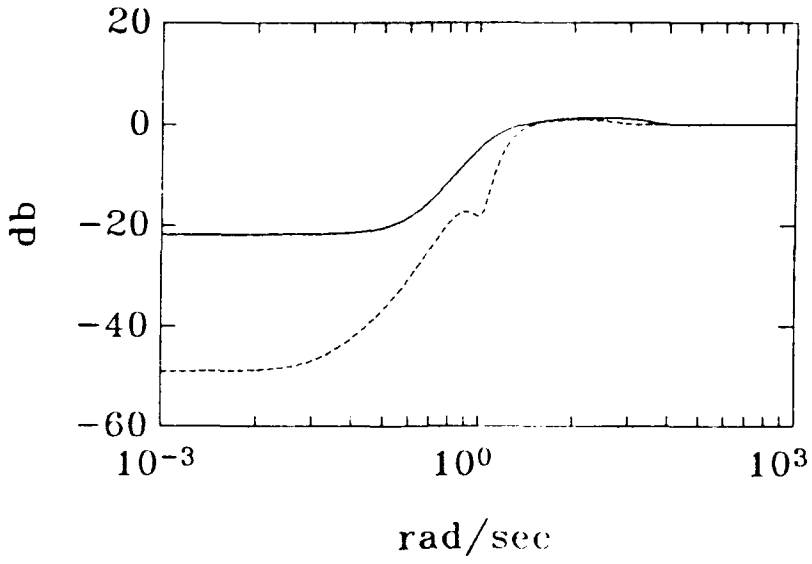

Figure 34 Sensitivity for Example 2 with 0.3 α shift

Figure 35 shows the control surface deflections required to perform a unit step β (sideslip angle) command input. The peak deflections and rates are similar to the unshifted case.

Figure 36 shows the control surface deflections required to perform a unit step ϕ (roll angle) command input. Here the peak deflection has increased to 0.8 degrees (from 0.4) and the rate has increased to around 30 degrees per second (from 20). This is still reasonable, but it is a lot greater than the unshifted case. The system must perform faster so more control power is required.

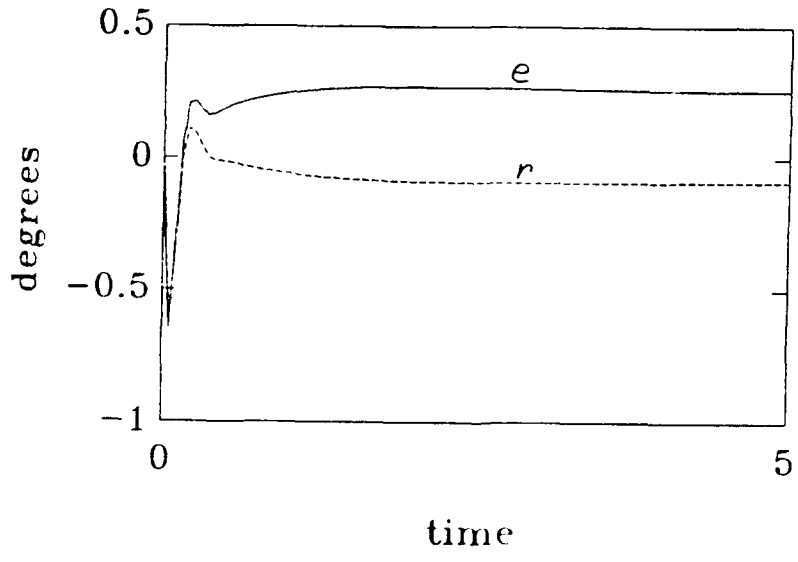

Figure 35 Control usage for unit step β command

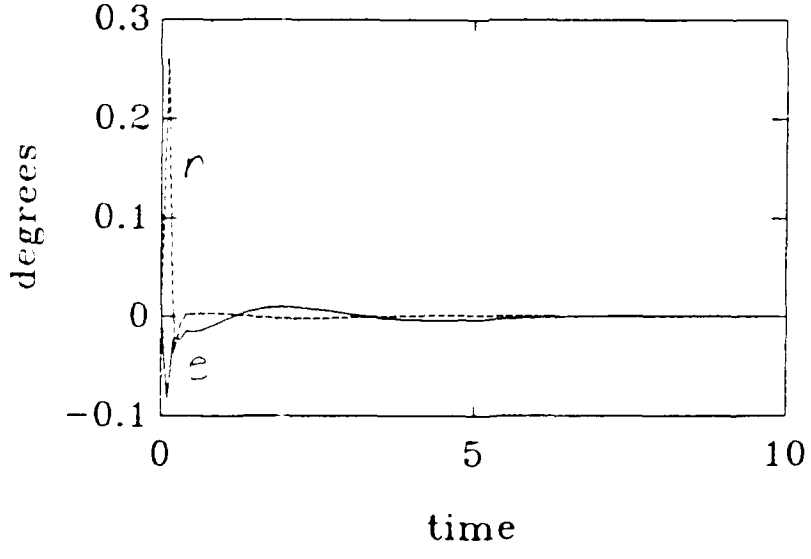

Figure 36 Control usage for a unit step ϕ command

Figure 37 shows how the system responds to a unit step β disturbance. This is where the penalty for the α shift begins to become apparent. The system responds much faster and the damping is increased, but it does not completely reject the disturbance. The steady state value is about 0.08 rather than the desired value of zero.

Figure 38 is the ϕ disturbance response. This is a vast improvement over the unshifted case. The oscillations damp out in less than 10 seconds (compared to 30) and the response has no steady state error.

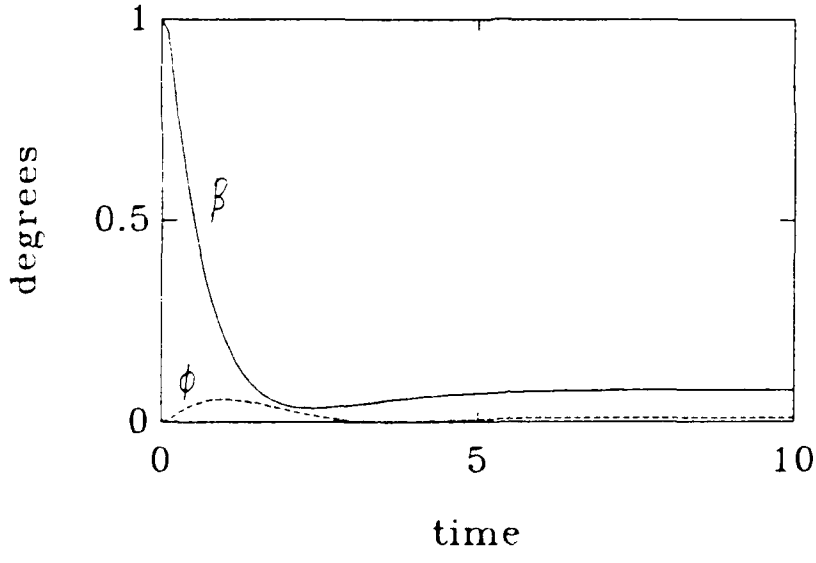

Figure 37 Rejecting a unit step β disturbance

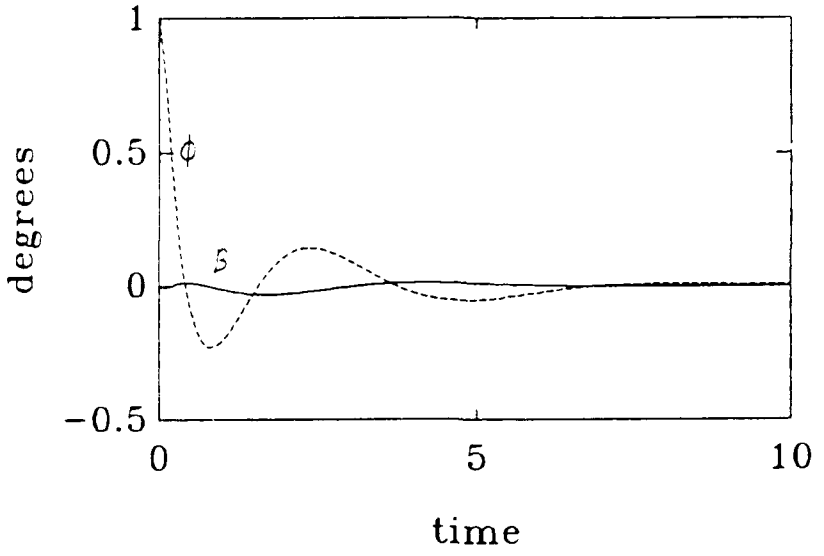

Figure 38 Rejecting a unit step ϕ disturbance

Figure 39 shows the response to a unit step β command input. Again the speed of the system has increased over the unshifted case, but the steady state has an error in it. The final value is about 0.92 rather than 1.

Figure 40 is the ϕ response. Here there is a major improvement over the unshifted case. The oscillations damp out in about 8 seconds (compared to 30) and the system has no steady state error.

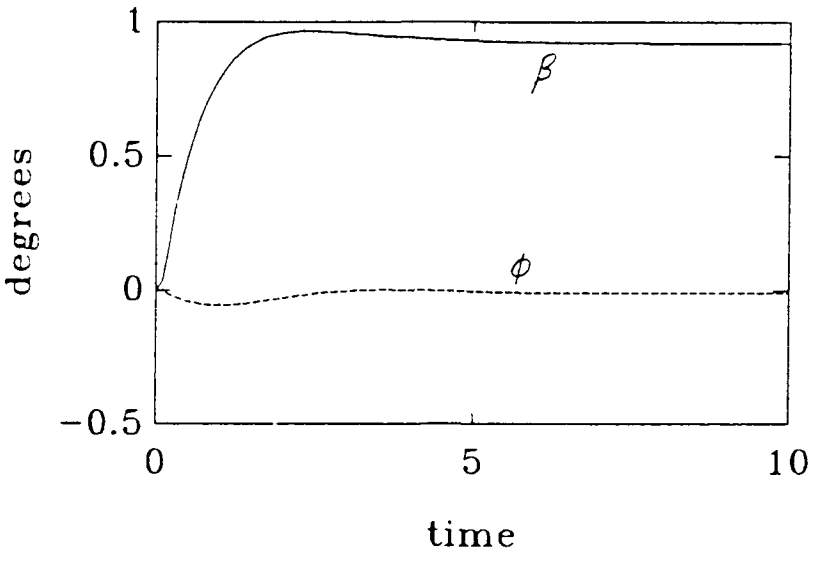

Figure 39 System response to a unit step β command input

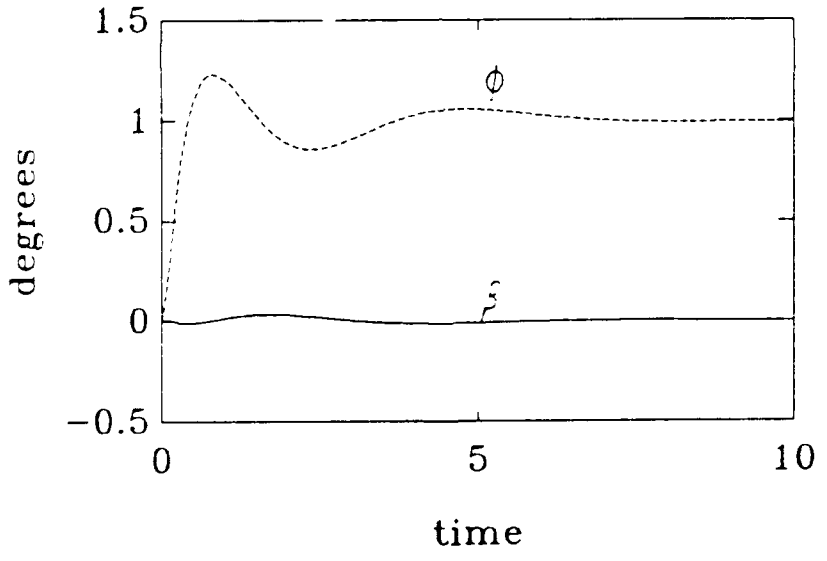

Figure 40 System response to a unit step ϕ command input

Table 7 shows the low frequency poles. Again the system has an additional 12 poles and 8 zeros beyond -10.

Table 7 Closed-loop poles and zeros

poles	zeros
-0.56401	0.18842 ± 1.0511 i
-1.0769 ± 0.32181 i	-0.035987
-1.0769 ± 0.32180 i	-0.36400 ± 0.90850 i
-0.78842 ± 1.0511 i	-0.52713 ± 0.13156 i
-3.2503	-0.73613
	-3.2503
	-3.2503

In Figure 41 the positions of the poles and zeros are shown graphically. Note how the poorly damped poles in the unshifted case have moved much farther into the LHP.

The open-loop poles at 0.18842 ± 1.0511i have been moved to their mirror image location across the shifted imaginary axis at -0.3 to -0.78842 ± 1.0511i. This greatly increases the damping of the system.

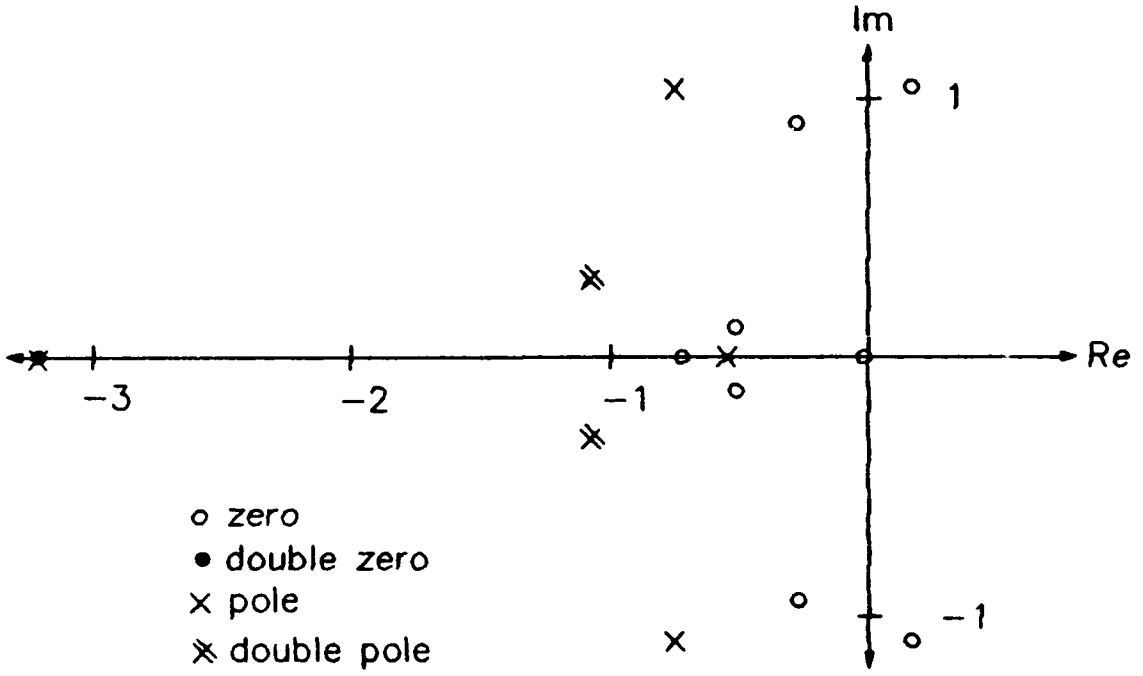

Figure 41 Poles and zeros for an α shift of 0.3

One other interesting point that came from Example 2 was the lack of dependance on ρ. Even when ρ was lowered to 0.0001, giving the system virtually unlimited control power, the steady state error did not improve much for the shifted case. The degradation in performance after the α shift was not due to a lack of control power available, but rather due to the mathematics of the controller design.

8. Perturbing the Plant

Example 2 shows how H_2 compensator design moves unstable complex poles to their mirror image location across the imaginary axis, and then places zeros near them to limit the effect they will have. This process works well if the system model is accurate and does not change. Systems do, however, change with time and conditions, and no model is perfect. If the poles are not where the compensator expects them to be, the zeros will not cancel them, and the effects of these pole will increase. This chapter will look at the problem from Example 2 with two different perturbations on the A matrix. These perturbations may come from flying in a different flight condition (new altitude, different weight due to burned fuel, etc) or from modeling errors. In the perturbed cases, the compensator was designed for the original plant and then the loop was closed around the perturbed plant. The original A matrix is

$$A = \begin{pmatrix} -0.08527 & -0.0001423 & -0.9994 & 0.04141 & 0 & 0.1862 \\ -46.86 & -2.757 & 0.3896 & 0 & -124.3 & 128.6 \\ -0.4248 & -0.06224 & -0.6714 & 0 & -8.792 & -20.46 \\ 0 & 1 & 0.0523 & 0 & 0 & 0 \\ 0 & 0 & 0 & 0 & -20 & 0 \\ 0 & 0 & 0 & 0 & 0 & -20 \end{pmatrix} \tag{132}$$

Table 8 shows the eigenvalues of the original open-loop plant.

Table 8 Open-loop poles

Dutch Roll (unstable)	0.1884 ± 1.0511 i
Spiral Mode	-0.0360
Roll Convergence	-3.2503
Elevon Actuator	-20.0
Rudder Actuator	-20.0

8.1. Perturbation Number 1

The first perturbed A matrix was

$$A = \begin{pmatrix} -0.082610 & -0.00021019 & -0.9994 & 0.04141 & 0 & 0.1862 \\ -46.86 & -4.01[illegible] & 0.3896 & 0 & -124.3 & 128.6 \\ -0.020024 & -0.06224 & -0.6714 & 0 & -8.792 & -20.46 \\ 0 & 1 & 0.0523 & 0 & 0 & 0 \\ 0 & 0 & 0 & 0 & -20 & 0 \\ 0 & 0 & 0 & 0 & 0 & -20 \end{pmatrix} \quad (133)$$

This changed the open-loop poles to the ones listed in Table 9.

Table 9 Open-loop poles

Dutch Roll (unstable)	0.07223 ± 1.0727 i
Spiral Mode	-0.024969
Roll Convergence	-4.2800
Elevon Actuator	-20.0
Rudder Actuator	-20.0

8.1.1. Perturbation Number 1 with no α Shift.

The sensitivity changed significantly from the unperturbed case, but it is still acceptable. The two channels are no longer together and the upper singular value increased to above -100 db for low frequencies. The 2 norm has increased to 13.67 from 12.12 in the unperturbed, unshifted case. The control usage is very similar to the unperturbed case, but with a little more oscillation. The roll angle (ϕ) disturbance rejection and command following are also similar to the unperturbed case. The big change is in the sideslip (β) disturbance rejection and command following. They both go to an initial deflection of 3.5 (unit step input) and oscillate for almost 40 seconds. See Figures 42-48.

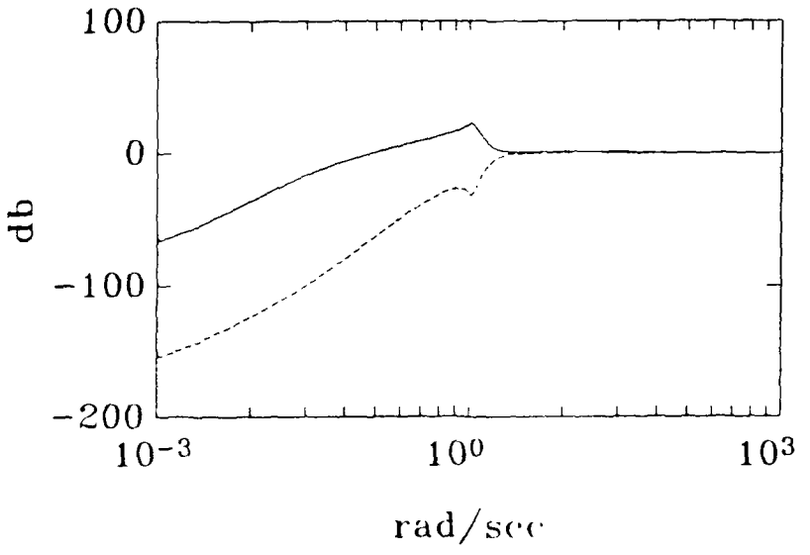

Figure 42 Sensitivity of perturbation 1 with no shift

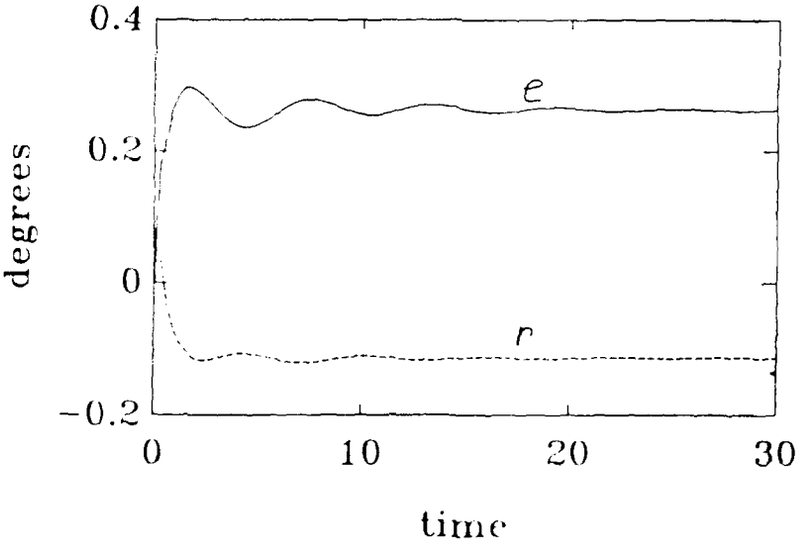

Figure 43 Control power required for a unit step β command

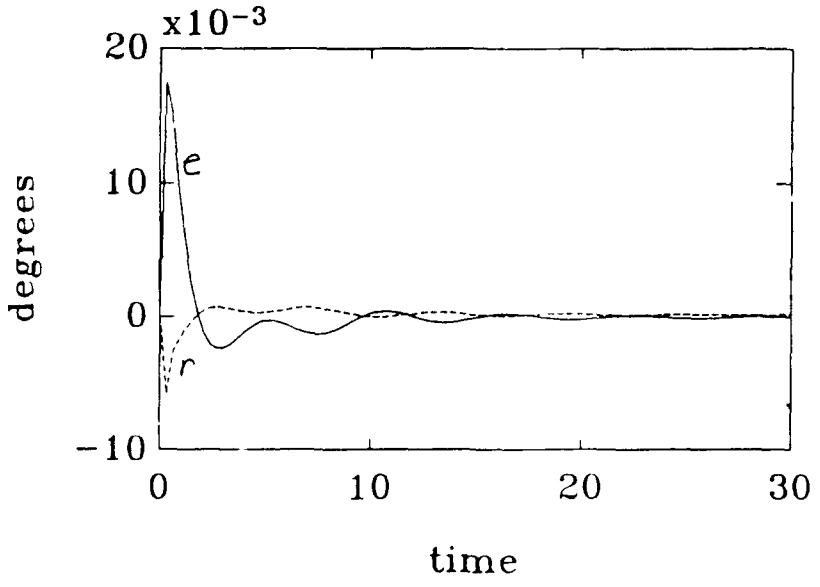

Figure 44 Control power required for a unit step ϕ command

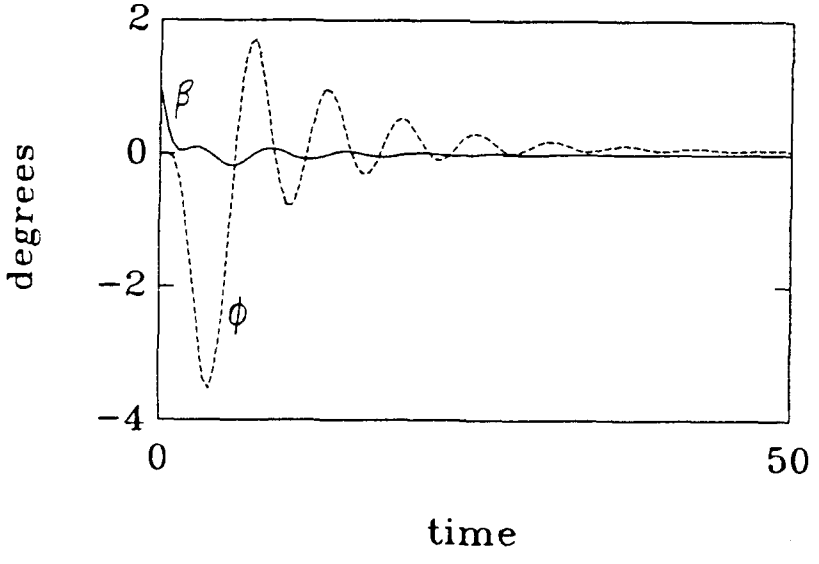

Figure 45 Rejecting a unit step β disturbance

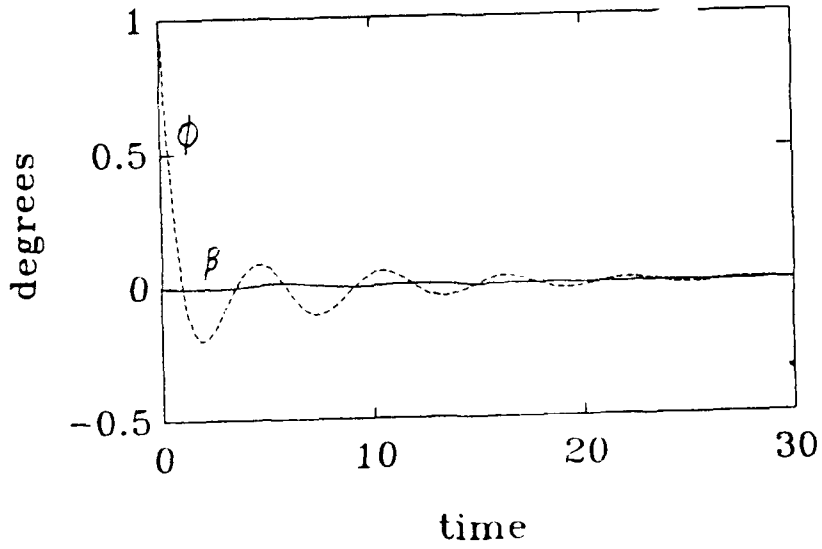

Figure 46 Rejecting a unit step ϕ disturbance

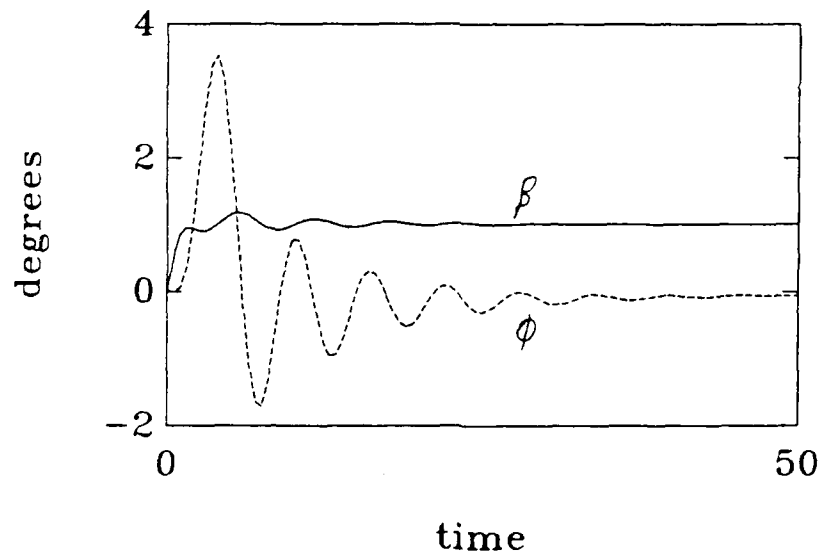

Figure 47 System response to a unit step β command input

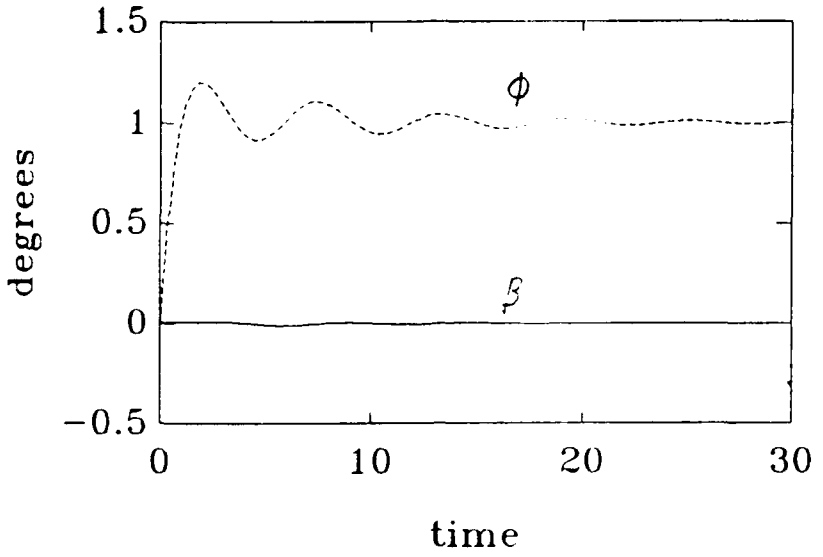

Figure 48 System Response to a unit step ϕ command input

8.1.2. Perturbation Number 1 with 0.3 α Shift.

Here the sensitivity has degraded to about -5 db at low frequencies. The 2 norm is almost the same as the unperturbed case with 0.3 α shift. It has increased from 17.52 to 17.53. Again, control usage is very similar to the unperturbed case. As in the perturbed, unshifted case the ϕ disturbance rejection and command following are very good. The big problem is in the β steady state error. The huge deflections from the unshifted case have been largely removed, but the steady state values for the unit step β

disturbance are around 0.2 and -0.4. The steady state values for a unit step β command are 0.8 and 0.4. The response reaches the final values for both β disturbance rejection and β command following much faster (around 10 seconds) but the final values are not what we want (see Figures 49-55)

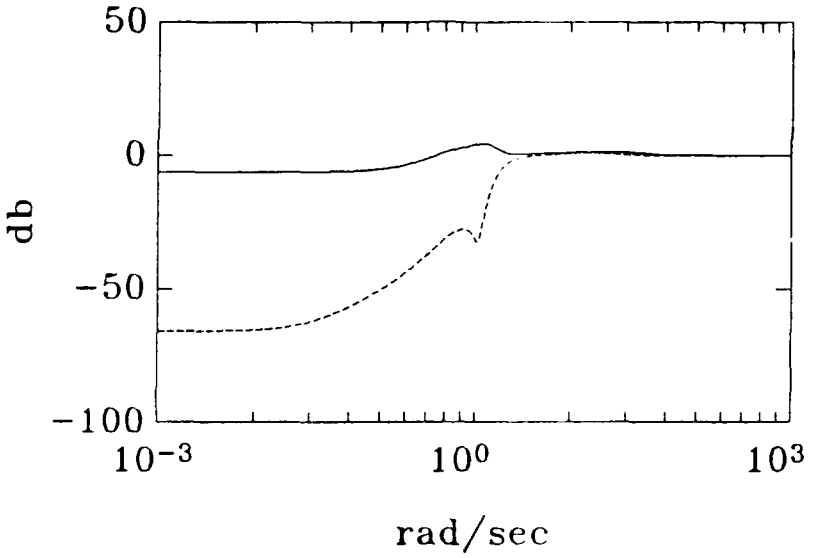

Figure 49 Sensitivity of perturbation 1 with 0.3 shift

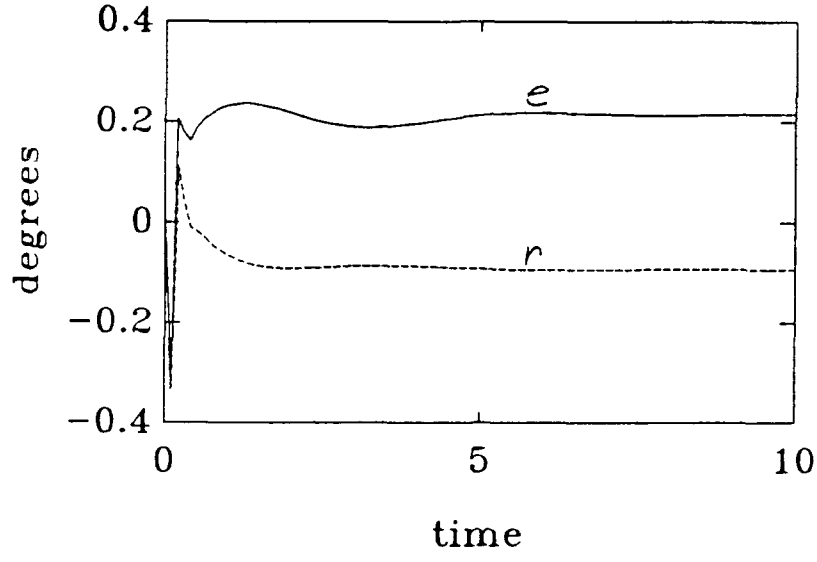

Figure 50 Control power required for a unit step β command

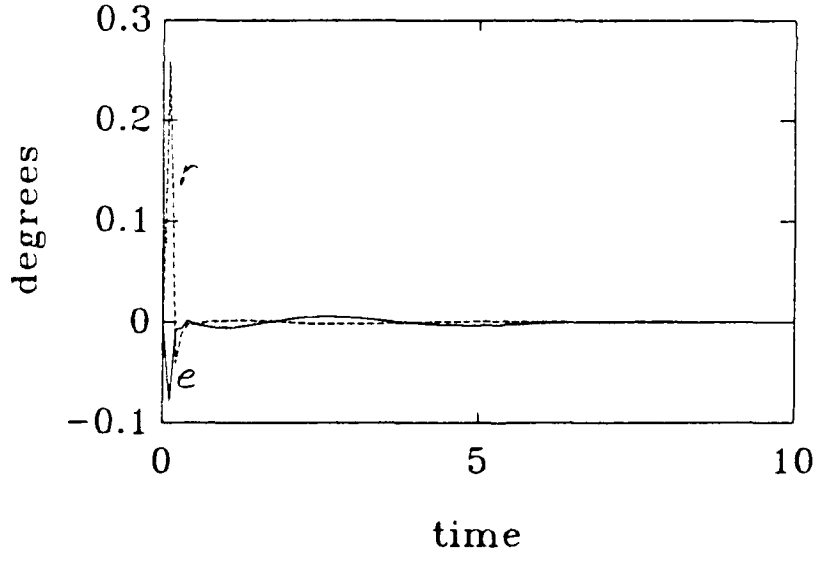

Figure 51 Control power required for a unit step ϕ command

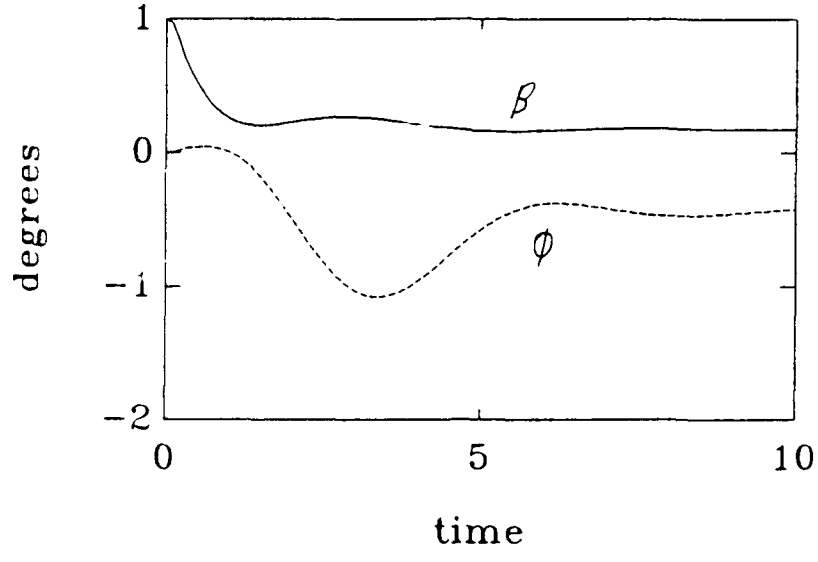

Figure 52 Rejecting a unit step β disturbance

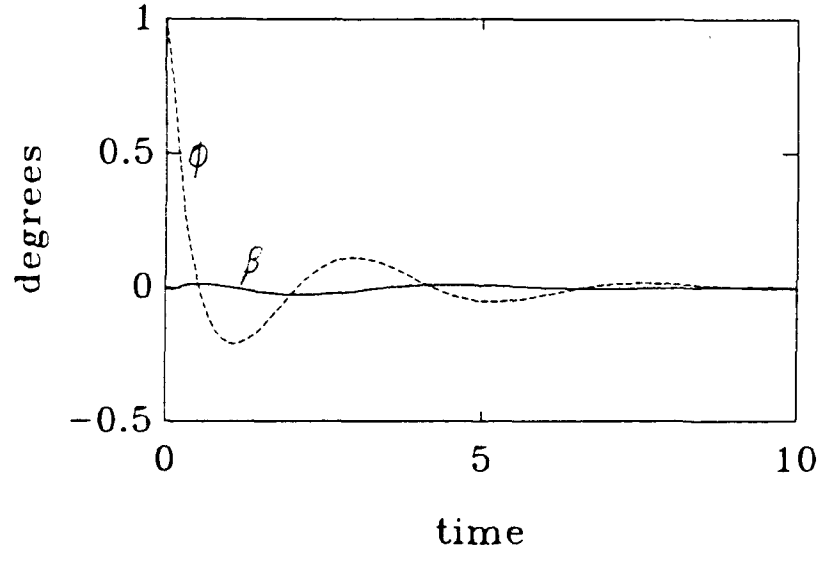

Figure 53 Rejecting a unit step ϕ disturbance

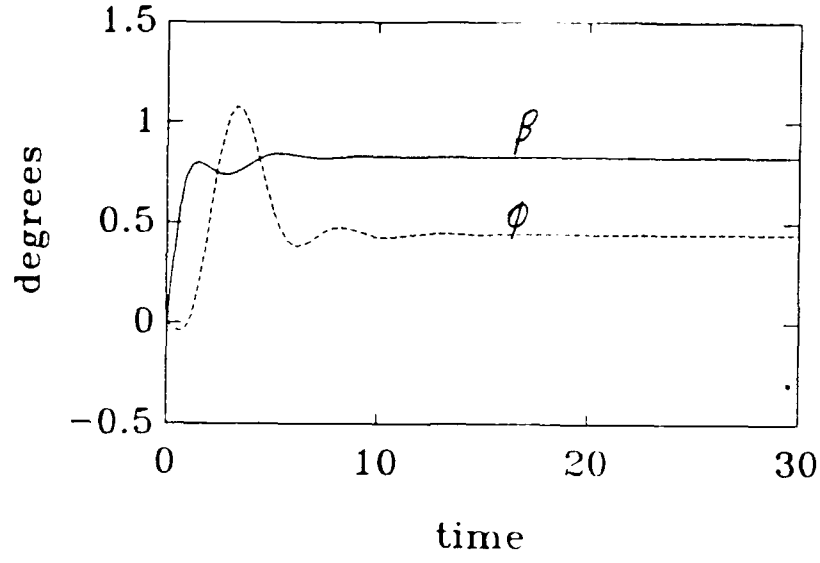

Figure 54 System response to a unit step β command input

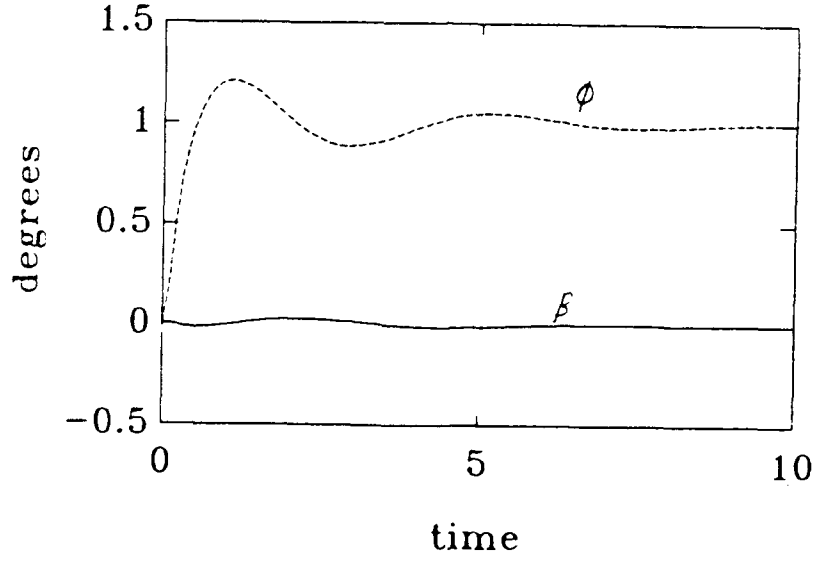

Figure 55 System response to a unit step ϕ command input

8.2. Perturbation Number 2

The results for the first perturbation are questionable as to whether the α shift is an improvement. The system does damp out much faster, but the steady state values are very poor in some cases. Consider, however, what happens when the plant is perturbed to a different value. The following is the second perturbed plant

$$A = \begin{pmatrix} -0.082610 & -0.00021019 & -0.9994 & 0.04141 & 0 & 0.1862 \\ -46.86 & -5.7815 & 0.3896 & 0 & -124.3 & 128.6 \\ -0.020024 & -0.06224 & -0.6714 & 0 & -8.792 & -20.46 \\ 0 & 1 & 0.0523 & 0 & 0 & 0 \\ 0 & 0 & 0 & 0 & -20 & 0 \\ 0 & 0 & 0 & 0 & 0 & -20 \end{pmatrix} \tag{134}$$

The eigenvalues for this plant are listed in Table 10.

Table 10 Open-loop poles

Dutch Roll (unstable)	0.006979 ± 0.91767 i
Spiral Mode	-0.024754
Roll Convergence	-5.9205
Elevon Actuator	-20.0
Rudder Actuator	-20.0

This is not much of a change from the first perturbation, but the closed-loop system with no α shift is now unstable. Any input or disturbance results in an unstable output. Using an α shift of 0.3, however, results in a stable closed-loop system. The results are very similar to the shifted case of perturbation number 1. They may have poor disturbance rejection and tracking in some channels, but they are definitely better than the unstable results for the unshifted case. Table 11 shows a summary the effects of perturbing the A matrix.

Table 11 Perturbing the A matrix

	Perturbation 1		Perturbation 2	
α shift	0	0.3	0	0.3
2 norm	13.67	17.53	∞	17.52
β dist. error (%)	0	40	u	40
β dist. time (sec)	50	12	n	20
ϕ dist. error (%)	0	0	s	0
ϕ dist. time (sec)	25	10	t	15
β track error (%)	0	40	a	40
β track time (sec)	50	12	b	20
ϕ track error (%)	0	0	l	0
ϕ track time (sec)	25	10	e	15

9. Results and Conclusions

Overall, the α shift did exactly what it was designed to do. It shifted all the closed-loop poles left of a vertical line some distance α from the imaginary axis. It also increased the damping of complex poles very near the imaginary axis. There were, however, significant reductions in the steady state performance.

9.1. Summarizing the Example Problems

Example 1 showed how the system responded as the α shift crossed each pole or zero. Shifting across a pole (making the system "unstable") or zero (making the system "nonminimum phase") caused a major decrease in the performance. The low frequency sensitivity increased, the control usage increased, and the steady state error for disturbance rejection and command following increased. This was reflected in drastic increases in both the 2 and ∞ norm. Damping was not a factor in Example 1, but it did show the desired increase in the speed of response.

Example 2 was a more interesting test of the method. In this example there were very lightly damped poles in the open-loop system. The α shift did considerably increase the

closed-loop damping of these poles. The open-loop plant was unstable, with a complex pair just right of the imaginary axis. Standard H_2 optimization moved these poles to roughly their mirror image locations in the left half plane. This stabilized the system, but these poles had very poor damping. The time response had oscillations for more than 20 seconds.

H_2 optimization with an α shift moved the open-loop unstable poles to their mirror image locations across the shifted imaginary axis. In effect this gave double the shift. The α shift dramatically increased the damping of the closed-loop system. The time response settled out in less than 10 seconds. The cost for this increased damping was mostly in the steady state error. There was approximately an eight percent error in both disturbance rejection and command following for one of two inputs. The other input still had no steady state error. An additional cost was a minor increase in the control power required.

Chapter 8 showed how the α shift increased the robustness of the closed-loop system. The A matrix of the plant was perturbed to produce two new A matrices, representative of two off-nominal fight conditions. The

compensator designed using an α shift was able to stabilize larger variations in the A matrix than standard H_2 optimization.

9.2. Conclusions

The α shift is basically another design variable, like ρ and W_s. It is most useful for systems that have closed-loop poles near the imaginary axis. It will increase the speed of response of the closed-loop system, and for lightly damped poles near the imaginary axis it will increase the damping ratio significantly. The α required is dependant on the particular system. Due to the tendency of H_2 and H_∞ optimization to move unstable poles to their mirror image, the benefit from an α shift is double what would be expected. The penalty for using an α shift can be significant. Moving all the poles away from the origin removes any integral action that may have been in the system. The steady state error can increase dramatically, especially as α get large.

9.2.1. Areas for Further Study.

The first thing to do would be to reproduce the results from Example 2 using H_∞ optimization. Most likely, they would be similar to the H_2 case, but may be worth

considering.

Next, it would be very beneficial to get the sensitivity, disturbance rejection, and command following of the unshifted case to carry over to the shifted case. There are several possible methods for doing this. The easiest things to try would be to adjust the weighting factors W_e and W_u. Increasing the gain on W_e and extending the bandwidth to around 10 rad/sec may help. For W_u it might be worth looking at a diagonal weighting, penalizing the control usage differently in each channel. If neither of these work, one could consider adding an additional outer loop with integral action.

The most important follow on work would be to derive the state space equations for the ζ rotation. This would move the lightly damped poles away from the imaginary axis without moving the poles near the origin that cause the loss of integral action. It is unlikely that the ζ rotation will work out as simply as the α shift, but it would be worth the effort.

Finally, a combined shift of the form shown in Figure 56 could be derived. The combined transformation shown in Chapter 4 does not guarantee a specific damping ratio. The new y axis is no longer rotated about the origin, but about

some point α from the origin. The shift in Figure 56 would increase the complexity of the transformation, however, because only a portion of the rotated axis is shifted, and the shift is not constant for all values of y.

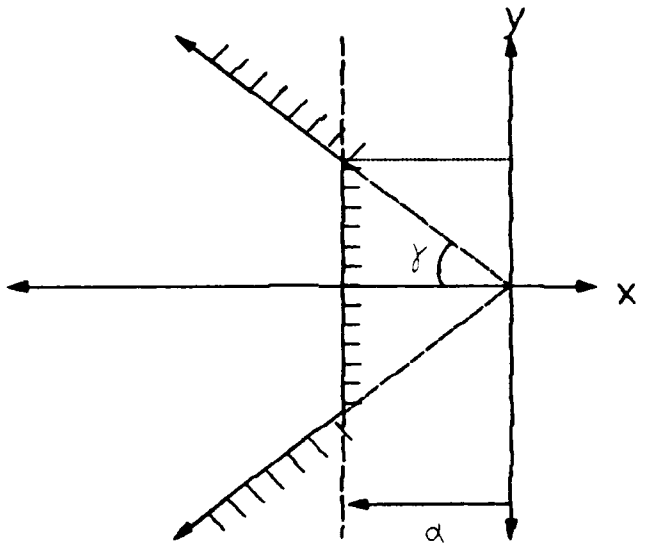

Figure 56 Combined s-plane transformation

Bibliography

1. Amin, M. H. "Optimal Pole Shifting for Continuous Multivariable Linear Systems," International Journal of Control, 41: 701-707, 1985.

2. Anderson, B. D. O. and J. B. Moore. Linear Optimal Control. Englewood Cliffs: Prentice Hall, 1971.

3. Anderson, B. D. O. and J. B. Moore. "Linear System Optimization with Prescribed Degree of Stability," Proc. IEE, 116: 2083-2087, December 1969.

4. Daily, R. Lane. "Lecture Notes for the Workshop on H_∞ and μ Methods for Robust Control," 1990 American Control Conference. San Diego, California, May 1990.

5. Doyle, John C. and Keith Glover. "State-Space Solutions to Standard H_2 and H_∞ Control Problems," IEEE Transactions on Automatic Control, AC-34: 831-846, August 1989.

6. Francis, Bruce A. "Lecture Notes in Control and Information Sciences,", Springer Verlag, 1986

7. Kawasaki, Naoya and Etsujiro Shimemura. "Determining Quadratic Weighting Matrices to Locate Poles in a Specified Region," Automatica, 19: 557-560, 1983.

8. Kwakernaak, Huibert and Raphael Sivan. Linear Optimal Control Systems. New York: Wiley-Interscience, 1972.

9. Olivier, Philip D. "A Constrained Optimal Control Problem," IEEE Transactions on Automatic Control, AC-29: 53-54, January 1984.

10. Ridgely, D. Brett and Siva S. Banda. Introduction To Robust Multivariable Control. AFWAL-TR-85-3102. Wright-Patterson AFB: AFSC, February 1986.

11. Shieh, Leang S. et al. "Linear Quadratic Regulators with Eigenvalue Placement in a Specified Region," Automatica, 24: 819-823, 1988.

12. Shieh, Leang S. et al. "Linear Quadratic Regulators with Eigenvalue Placement in a Vertical Strip," IEEE Transactions on Automatic Control, AC-31: 241-243, March 1986.

Vita

Captain Michael J. Mares [redacted] He graduated from Lakeville High School in Lakeville, Minnesota in 1982 and attended the U. S. Air Force Academy, graduating with a Bachelor of Science in Astronautical Engineering in May 1986. Upon graduation, he received a regular commission in the USAF and served his first tour of duty at Edwards AFB, California. He began as a Test Engineer for the 6595 Test and Evaluation Group, Antisatellite Operating Location where he directed testing on the F-15 launched Antisatellite missile. In April 1987 he was chosen to serve as Chief of the 6595 Test and Evaluation Group, Antisatellite Operating Location. In May 1989 he entered the School of Engineering, Air Force Institute of Technology.

[redacted]

REPORT DOCUMENTATION PAGE

Form Approved
OMB No 0704-0188

1. AGENCY USE ONLY (Leave blank)	2. REPORT DATE	3. REPORT TYPE AND DATES COVERED
	December 1990	Master's Thesis

4. TITLE AND SUBTITLE
H2 AND H INFINITY OPTIMIZATION WITH A RESTRICTED REGION OF STABILITY

5. FUNDING NUMBERS

6. AUTHOR(S)
Michael J. Mares, Captain, USAF

7. PERFORMING ORGANIZATION NAME(S) AND ADDRESS(ES)
Air Force Institute of Technology
WPAFB OH 45433-6583

8. PERFORMING ORGANIZATION REPORT NUMBER
AFIT/GAE/ENY/90D-15

9. SPONSORING MONITORING AGENCY NAME(S) AND ADDRESS(ES)
Dr. Siva S. Banda
WRDC/FIGC
WPAFB OH 45433

10. SPONSORING MONITORING AGENCY REPORT NUMBER

11. SUPPLEMENTARY NOTES

12a DISTRIBUTION AVAILABILITY STATEMENT
Approved for public release; distribution unlimited

12b DISTRIBUTION CODE

13. ABSTRACT *(Maximum 200 words)*

Many modern control design methods, such as H2 and Hinfinity optimization, guarantee that the closed-loop system will be stable. To make further use of this guatantee, the portion of the s-plane considered to be stable is restricted to a region left of a vertical line some distance alpha from the imaginary axis. This alpha shift was accomplished in the state space equations, so standard computational tools still work. Now the system is not only guaranteed to be stable, but also has some guaranteed speed for the time response. The equations for guaranteeing some arbitrary damping ratio were also derived in Cartesian coordinates, but only the alpha shift was put into the state space equation form and tested. The alpha shift increased the speed of the sytem, as expected. An additional benefit was increasing the damping of lightly damped poles. The cost for doing this was an increase in the steady state error and an increase in the control power required.

14. SUBJECT TERMS	15. NUMBER OF PAGES
Control Theory, Control, Theory, Control Systems, Flight Control Systems, Command and Control Systems, Linear Programming, Optimization	112
	16. PRICE CODE

17. SECURITY CLASSIFICATION OF REPORT	18. SECURITY CLASSIFICATION OF THIS PAGE	19. SECURITY CLASSIFICATION OF ABSTRACT	20. LIMITATION OF ABSTRACT
Unclassified	Unclassified	Unclassified	UL